Supporting Information

Impact of Metal and Heteroatom Identities in the Hydrogenolysis of C–X Bonds (X = C, N, O, S, and Cl)

Abdulrahman S. Almithn[1,2] and David D. Hibbitts[1]*

[1]Department of Chemical Engineering, University of Florida, Gainesville, Florida, 32611, United States

[2]Department of Chemical Engineering, King Faisal University, Al-Ahsa, 31982, Saudi Arabia

*Corresponding author: hibbitts@che.ufl.edu

Table of Contents

List of Tables

List of Figures

S1. Details of Density Functional Calculations of Thermochemical Properties

Close-packed metal surfaces—(111) surfaces for FCC metals and (001) surfaces for HCP metals—were modeled as 3 × 3 periodic lattices with four layers orthogonal to the surface and 10 Å of vacuum separating slabs (Fig. S1); the bottom two layers were fixed in their bulk positions and the top two layers were relaxed.

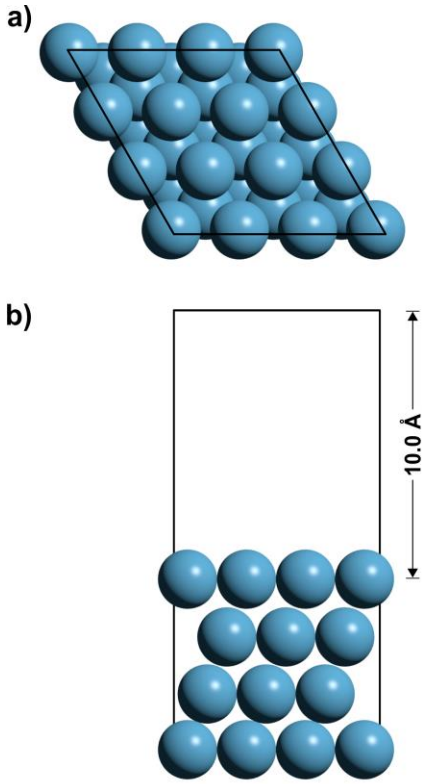

Figure S1. (a) Top and (b) side views of the metal 3×3 (111) surface. The bottom two layers were fixed at their bulk positions during geometric convergence.

Frequency calculations were performed on gas phase molecules and all optimized adsorbed species to determine zero-point vibrational energies (ZPVE), and vibrational, translational and rotational enthalpy and free energy. These terms were then used, together with electronic energies (E_0, provided by VASP), to estimate enthalpies (H)

$$H = E_0 + \mathrm{ZPVE} + H_{\mathrm{vib}} + H_{\mathrm{trans}} + H_{\mathrm{rot}} \quad \text{(S1)}$$

and free energies (G)

$$G = E_0 + \mathrm{ZPVE} + G_{\mathrm{vib}} + G_{\mathrm{trans}} + G_{\mathrm{rot}} \quad \text{(S2)}$$

for reactants, products, and transition states at 593 K (the temperature at which ethane hydrogenolysis rates were measured). The entropy can be determined for a state with a known H and G at a given T:

$$S = \frac{H - G}{T} \quad \text{(S3)}$$

For calculations which include a periodic metal surface or a metal half-particle, the translational and rotational degrees of freedom are hindered and treated as vibrations. DFT-derived vibrational frequencies can then be used to determine the ZPVE, H_{vib}, and G_{vib}

$$ZPVE = \sum_i (½ \nu_i h) \tag{S4}$$

$$H_{vib} = \sum_i \left(\frac{\nu_i h e^{\frac{-\nu_i h}{kT}}}{1 - e^{\frac{-\nu_i h}{kT}}} \right) \tag{S5}$$

$$G_{vib} = \sum_i \left(-kT \ln \frac{1}{1 - e^{\frac{-\nu_i h}{kT}}} \right) \tag{S6}$$

For gaseous molecules, translational and rotational enthalpies and free energies were also computed from statistical mechanics:

$$H_{trans} = \frac{5}{2} kT \tag{S7}$$

$$H_{rot,linear} = kT \tag{S8}$$

$$H_{rot,nonlinear} = \frac{3}{2} kT \tag{S9}$$

$$G_{trans} = -kT \ln\left[\left(\frac{2\pi MkT}{h^2} \right)^{3/2} V \right] \tag{S10}$$

$$G_{rot} = -kT \ln\left[\frac{\pi^{1/2}}{\sigma} \left(\frac{T^3}{\theta_x \theta_y \theta_z} \right)^{1/2} \right] \tag{S11}$$

$$\theta_i = \frac{h^2}{8\pi^2 I_i k} \tag{S12}$$

where I_i is the moment of inertia about axes *x*, *y* or *z* and σ is the symmetry number of the molecule (2 for H_2 and 6 for C_2H_6). Equations S7–S12 obtained from: McQuarrie, D. A.; Statistical Mechanics; Sausolito, CA.

S2. Effective free energy barriers

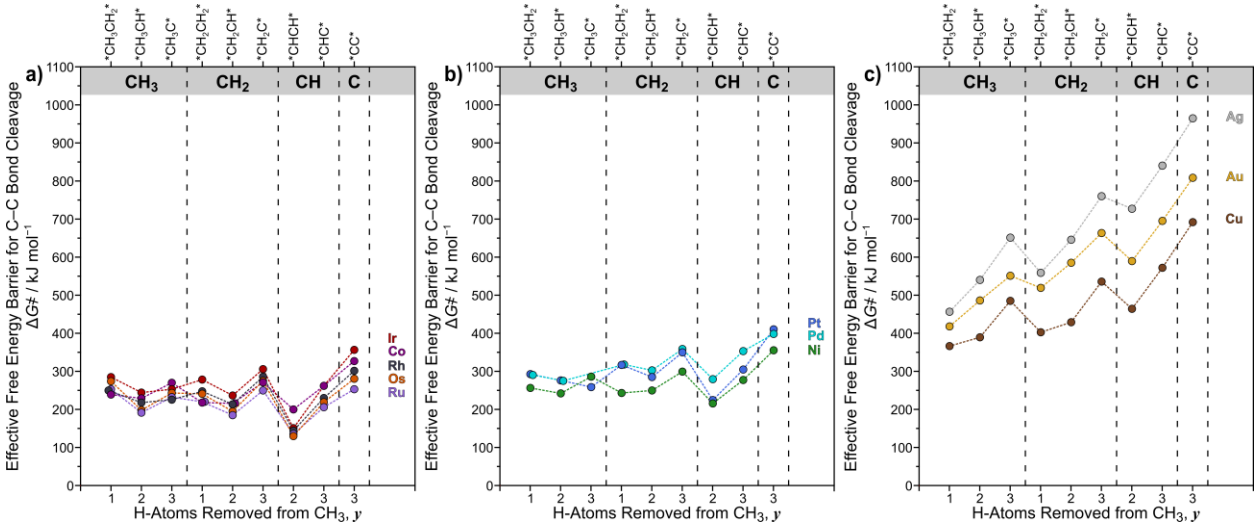

Figure S2. Effective free energy barriers for C–C bond cleavage in ethane-derived intermediates on a) Groups 8–9, b) Group 10, and c) Group 11 metals (450 K, 1 bar H_2). Dashed lines are drawn to guide the eye.

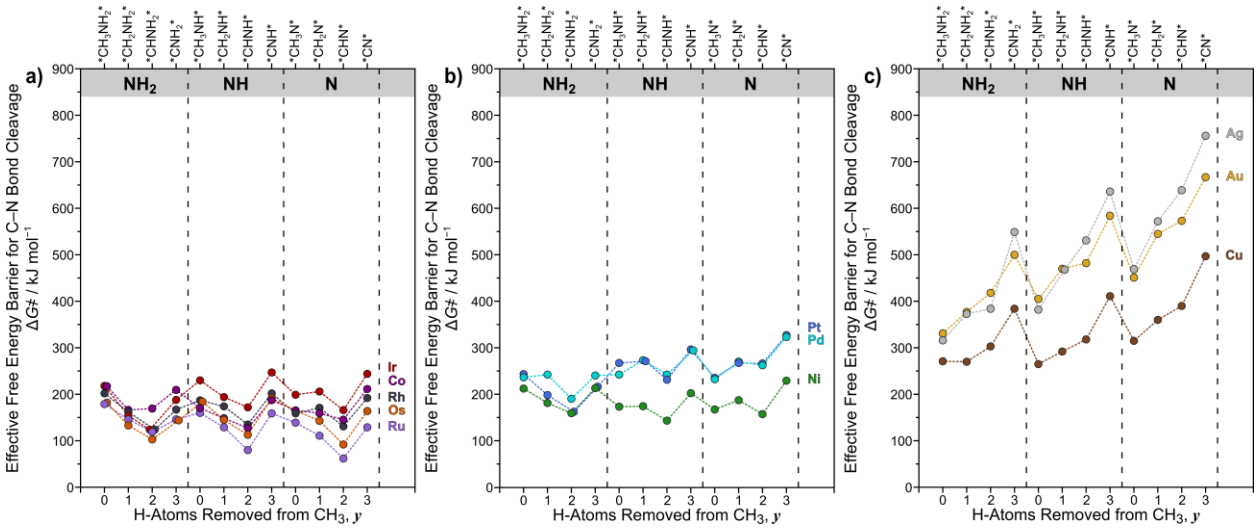

Figure S3. Effective free energy barriers for C–N bond cleavage in methylamine-derived intermediates on a) Groups 8–9, b) Group 10, and c) Group 11 metals (450 K, 1 bar H_2). Dashed lines are drawn to guide the eye.

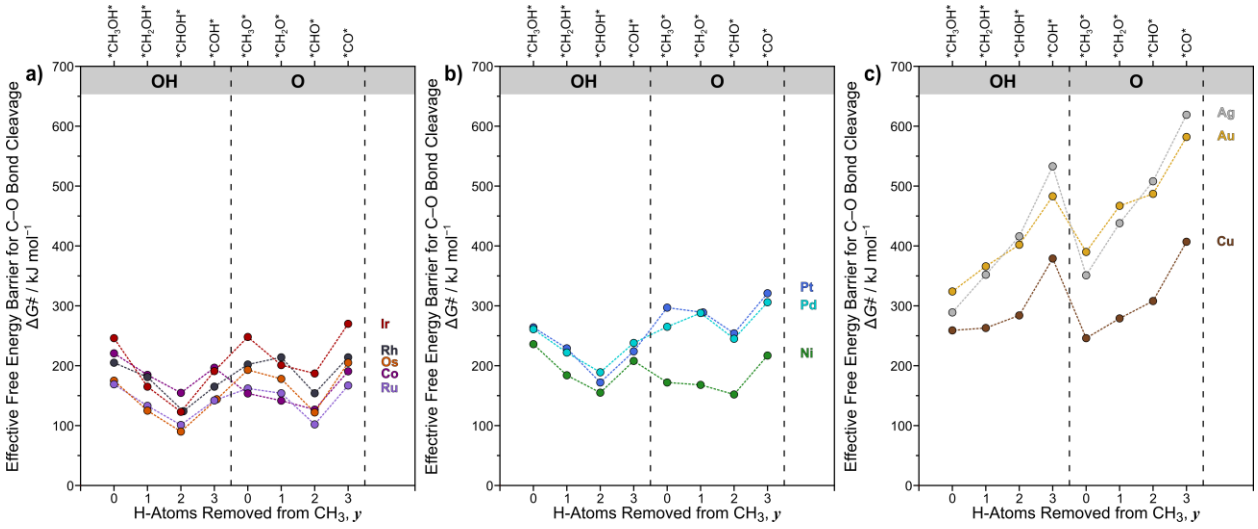

Figure S4. Effective free energy barriers for C–O bond cleavage in methanol-derived intermediates on a) Groups 8–9, b) Group 10, and c) Group 11 metals (450 K, 1 bar H_2). Dashed lines are drawn to guide the eye.

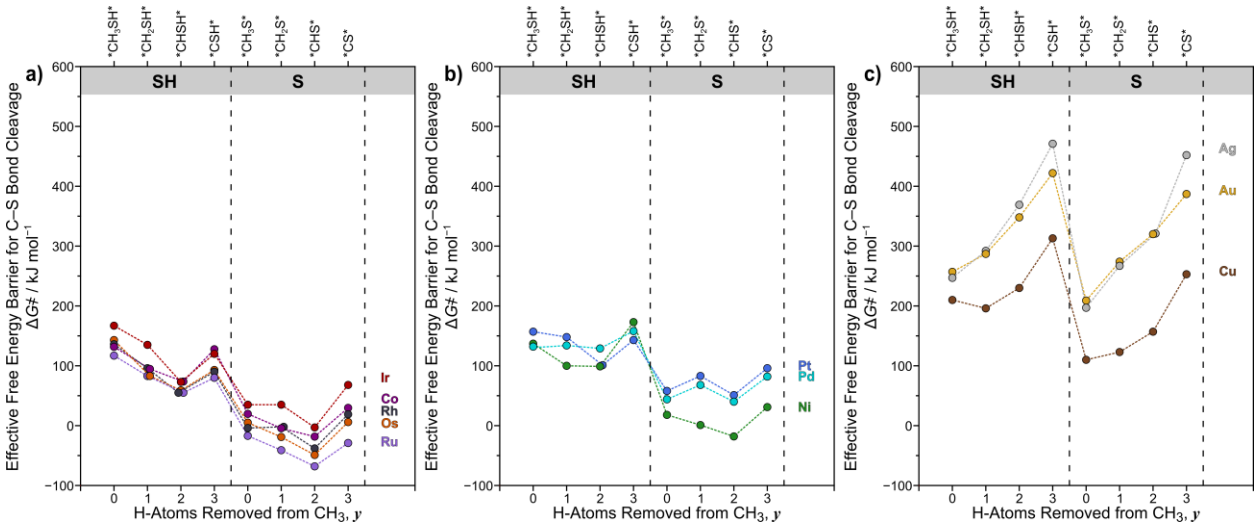

Figure S5. Effective free energy barriers for C–S bond cleavage in methanethiol-derived intermediates on a) Groups 8–9, b) Group 10, and c) Group 11 metals (450 K, 1 bar H_2). Dashed lines are drawn to guide the eye.

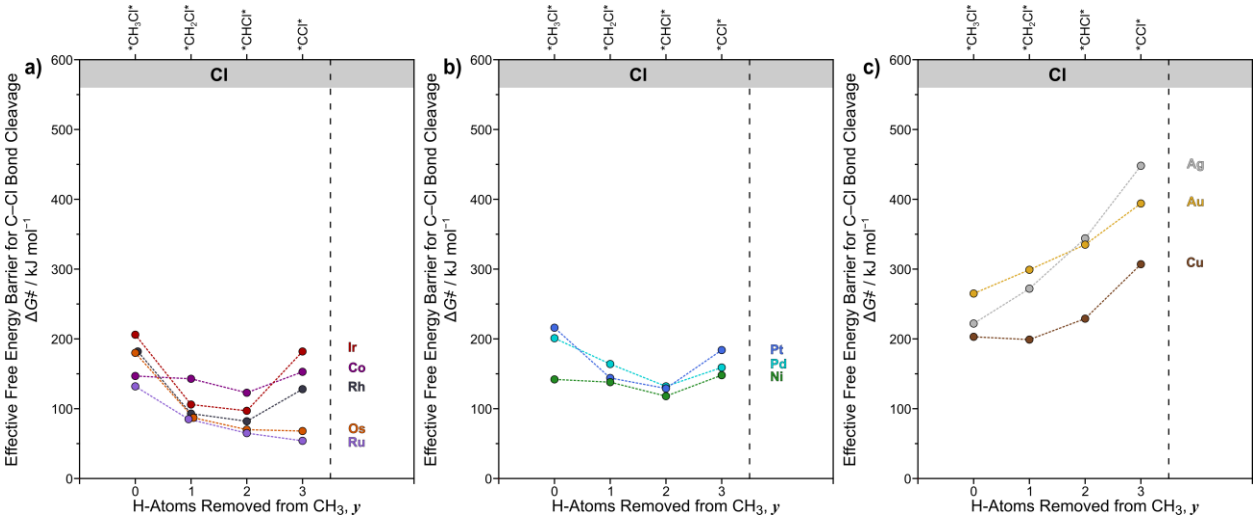

Figure S6. Effective free energy barriers ($\Delta G^{\ddagger}$) C–Cl bond cleavage in chloromethane-derived intermediates on a) Groups 8–9, b) Group 10, and c) Group 11 metals (450 K, 1 bar H_2). Dashed lines are drawn to guide the eye.

S3. Transition State Energies

Table S1. DFT-predicted effective barriers (Eqs. 1 and 3) for C–C activation at 450 K and 1 bar H_2

Catalyst	Reaction	$\Delta H^{\neq}$ kJ mol^{-1}	$\Delta G^{\neq}$ kJ mol^{-1}	$\Delta S^{\neq}$ J mol^{-1} K^{-1}
Ru(001)	$*CH_3CH_2* \rightarrow CH_3* + CH_2*$	195	230	-77
	$*CH_2CH_2* \rightarrow CH_2* + CH_2*$	187	200	-30
	$*CH_3CH* \rightarrow CH_3* + CH*$	157	174	-37
	$*CH_3C* \rightarrow CH_3* + C*$	224	211	29
	$*CH_2CH* \rightarrow CH_2* + CH*$	179	168	26
	$*CHCH* \rightarrow CH* + CH*$	155	123	72
	$*CH_2C* \rightarrow CH_2* + C*$	264	227	82
	$*CHC* \rightarrow CH* + C*$	249	187	139
	$*CC* \rightarrow C* + C*$	321	230	201
Os(001)	$*CH_3CH_2* \rightarrow CH_3* + CH_2*$	214	249	-80
	$*CH_2CH_2* \rightarrow CH_2* + CH_2*$	203	219	-36
	$*CH_3CH* \rightarrow CH_3* + CH*$	162	180	-42
	$*CH_3C* \rightarrow CH_3* + C*$	233	221	25
	$*CH_2CH* \rightarrow CH_2* + CH*$	184	177	15
	$*CHCH* \rightarrow CH* + CH*$	150	118	71
	$*CH_2C* \rightarrow CH_2* + C*$	288	250	85
	$*CHC* \rightarrow CH* + C*$	262	199	138
	$*CC* \rightarrow C* + C*$	345	255	201
Co(001)	$*CH_3CH_2* \rightarrow CH_3* + CH_2*$	201	230	-66
	$*CH_2CH_2* \rightarrow CH_2* + CH_2*$	200	209	-20
	$*CH_3CH* \rightarrow CH_3* + CH*$	214	220	-13
	$*CH_3C* \rightarrow CH_3* + C*$	286	261	56
	$*CH_2CH* \rightarrow CH_2* + CH*$	226	207	41
	$*CHCH* \rightarrow CH* + CH*$	228	191	82
	$*CH_2C* \rightarrow CH_2* + C*$	309	262	105
	$*CHC* \rightarrow CH* + C*$	317	253	142
	$*CC* \rightarrow C* + C*$	410	318	205
Rh(111)	$*CH_3CH_2* \rightarrow CH_3* + CH_2*$	191	227	-80
	$*CH_2CH_2* \rightarrow CH_2* + CH_2*$	207	225	-41
	$*CH_3CH* \rightarrow CH_3* + CH*$	188	198	-23
	$*CH_3C* \rightarrow CH_3* + C*$	219	205	32
	$*CH_2CH* \rightarrow CH_2* + CH*$	202	194	16
	$*CHCH* \rightarrow CH* + CH*$	168	131	82
	$*CH_2C* \rightarrow CH_2* + C*$	298	260	84
	$*CHC* \rightarrow CH* + C*$	270	209	136
	$*CC* \rightarrow C* + C*$	368	274	209
Ir(111)	$*CH_3CH_2* \rightarrow CH_3* + CH_2*$	220	259	-88
	$*CH_2CH_2* \rightarrow CH_2* + CH_2*$	235	253	-42
	$*CH_3CH* \rightarrow CH_3* + CH*$	211	222	-26
	$*CH_3C* \rightarrow CH_3* + C*$	243	230	28
	$*CH_2CH* \rightarrow CH_2* + CH*$	226	215	24

	CHCH → CH* + CH*	179	137	92
	CH_2C → CH_2* + C*	316	278	85
	CHC → CH* + C*	298	238	134
	CC → C* + C*	416	324	205
Ni(111)	*CH_3CH_2* → CH_3* + CH_2*	192	233	-91
	CH_2CH_2 → CH_2* + CH_2*	203	221	-41
	CH_3CH → CH_3* + CH*	203	220	-38
	CH_3C → CH_3* + C*	273	260	30
	CH_2CH → CH_2* + CH*	235	227	17
	CHCH → CH* + CH*	230	196	75
	CH_2C → CH_2* + C*	307	272	80
	CHC → CH* + C*	314	252	137
	CC → C* + C*	414	323	201
Pd(111)	*CH_3CH_2* → CH_3* + CH_2*	226	264	-83
	CH_2CH_2 → CH_2* + CH_2*	270	289	-42
	CH_3CH → CH_3* + CH*	240	250	-24
	CH_3C → CH_3* + C*	275	260	33
	CH_2CH → CH_2* + CH*	281	275	15
	CHCH → CH* + CH*	290	254	80
	CH_2C → CH_2* + C*	362	326	79
	CHC → CH* + C*	382	321	135
	CC → C* + C*	453	362	203
Pt(111)	*CH_3CH_2* → CH_3* + CH_2*	226	266	-89
	CH_2CH_2 → CH_2* + CH_2*	267	288	-45
	CH_3CH → CH_3* + CH*	240	251	-24
	CH_3C → CH_3* + C*	248	235	27
	CH_2CH → CH_2* + CH*	270	259	25
	CHCH → CH* + CH*	242	204	85
	CH_2C → CH_2* + C*	352	318	76
	CHC → CH* + C*	342	277	145
	CC → C* + C*	465	373	204
Cu(111)	*CH_3CH_2* → CH_3* + CH_2*	298	333	-78
	CH_2CH_2 → CH_2* + CH_2*	347	366	-43
	CH_3CH → CH_3* + CH*	345	354	-21
	CH_3C → CH_3* + C*	457	441	37
	CH_2CH → CH_2* + CH*	400	390	21
	CHCH → CH* + CH*	463	422	91
	CH_2C → CH_2* + C*	524	487	83
	CHC → CH* + C*	589	520	153
	CC → C* + C*	726	629	217
Ag(111)	*CH_3CH_2* → CH_3* + CH_2*	382	415	-73
	CH_2CH_2 → CH_2* + CH_2*	492	508	-35
	CH_3CH → CH_3* + CH*	484	491	-15
	CH_3C → CH_3* + C*	612	592	44
	CH_2CH → CH_2* + CH*	598	587	23
	CHCH → CH* + CH*	704	661	95

	*CH_2C^* → CH_2^* + C^*	738	691	104
	*CHC^* → CH^* + C^*	836	764	161
	*CC^* → C^* + C^*	982	877	233
Au(111)	*$CH_3CH_2^*$ → CH_3^* + CH_2^*	344	380	-81
	*$CH_2CH_2^*$ → CH_2^* + CH_2^*	453	472	-43
	*CH_3CH^* → CH_3^* + CH^*	427	442	-34
	*CH_3C^* → CH_3^* + C^*	518	501	38
	*CH_2CH^* → CH_2^* + CH^*	539	532	15
	*$CHCH^*$ → CH^* + CH^*	569	536	72
	*CH_2C^* → CH_2^* + C^*	638	603	78
	*CHC^* → CH^* + C^*	695	632	140
	*CC^* → C^* + C^*	828	735	206

Table S2. DFT-predicted effective barriers (Eqs. 1 and 3) for C–N activation at 450 K and 1 bar H_2

Catalyst	Reaction	$\Delta H^{\neq}$ kJ mol^{-1}	$\Delta G^{\neq}$ kJ mol^{-1}	$\Delta S^{\neq}$ J mol^{-1} K^{-1}
Ru(001)	*CN* → C* + N*	186	129	126
	CHN → CH* + N*	90	62	62
	CH_2N → CH_2* + N*	115	111	9
	CH_3N → CH_3* + N*	120	139	-43
	CNH → C* + NH*	192	159	72
	CHNH → CH* + NH*	77	80	-5
	CH_2NH → CH_2* + NH*	105	129	-53
	CH_3NH → CH_3* + NH*	109	160	-113
	CNH_2 → C* + NH_2*	153	146	15
	$CHNH_2$ → CH* + NH_2*	94	119	-55
	CH_2NH_2 → CH_2* + NH_2*	100	146	-103
	CH_3NH_2 → CH_3* + NH_2*	98	179	-178
Os(001)	*CN* → C* + N*	221	164	127
	CHN → CH* + N*	120	92	63
	CH_2N → CH_2* + N*	144	143	3
	CH_3N → CH_3* + N*	145	165	-44
	CNH → C* + NH*	221	192	63
	CHNH → CH* + NH*	111	113	-4
	CH_2NH → CH_2* + NH*	118	145	-61
	CH_3NH → CH_3* + NH*	131	184	-117
	CNH_2 → C* + NH_2*	149	144	11
	$CHNH_2$ → CH* + NH_2*	77	103	-58
	CH_2NH_2 → CH_2* + NH_2*	83	133	-111
	CH_3NH_2 → CH_3* + NH_2*	100	182	-184
Co(001)	*CN* → C* + N*	271	204	148
	CHN → CH* + N*	175	138	82
	CH_2N → CH_2* + N*	162	152	22
	CH_3N → CH_3* + N*	149	158	-20
	CNH → C* + NH*	218	180	85
	CHNH → CH* + NH*	125	120	12
	CH_2NH → CH_2* + NH*	123	141	-39
	CH_3NH → CH_3* + NH*	125	163	-84
	CNH_2 → C* + NH_2*	215	202	30
	$CHNH_2$ → CH* + NH_2*	151	162	-23
	CH_2NH_2 → CH_2* + NH_2*	118	159	-92
	CH_3NH_2 → CH_3* + NH_2*	152	210	-129
Rh(111)	*CN* → C* + N*	249	192	126
	CHN → CH* + N*	158	131	60
	CH_2N → CH_2* + N*	173	171	5
	CH_3N → CH_3* + N*	139	159	-45
	CNH → C* + NH*	231	202	64
	CHNH → CH* + NH*	132	135	-5
	CH_2NH → CH_2* + NH*	148	174	-58

	CH_3NH → CH_3* + NH*	135	187	-115
	CNH_2 → C* + NH_2*	171	167	10
	$CHNH_2$ → CH* + NH_2*	98	124	-58
	CH_2NH_2 → CH_2* + NH_2*	122	162	-89
	CH_3NH_2 → CH_3* + NH_2*	122	202	-177
Ir(111)	*CN* → C* + N*	301	244	126
	CHN → CH* + N*	192	166	59
	CH_2N → CH_2* + N*	206	206	-1
	CH_3N → CH_3* + N*	178	199	-46
	CNH → C* + NH*	274	247	60
	CHNH → CH* + NH*	169	172	-7
	CH_2NH → CH_2* + NH*	167	194	-60
	CH_3NH → CH_3* + NH*	177	230	-117
	CNH_2 → C* + NH_2*	195	188	15
	$CHNH_2$ → CH* + NH_2*	97	124	-60
	CH_2NH_2 → CH_2* + NH_2*	113	154	-92
	CH_3NH_2 → CH_3* + NH_2*	135	218	-183
Ni(111)	*CN* → C* + N*	285	230	122
	CHN → CH* + N*	184	158	58
	CH_2N → CH_2* + N*	188	188	-1
	CH_3N → CH_3* + N*	147	168	-46
	CNH → C* + NH*	230	203	59
	CHNH → CH* + NH*	142	144	-4
	CH_2NH → CH_2* + NH*	148	175	-61
	CH_3NH → CH_3* + NH*	122	174	-115
	CNH_2 → C* + NH_2*	216	214	3
	$CHNH_2$ → CH* + NH_2*	136	160	-53
	CH_2NH_2 → CH_2* + NH_2*	132	182	-111
	CH_3NH_2 → CH_3* + NH_2*	140	213	-162
Pd(111)	*CN* → C* + N*	388	324	142
	CHN → CH* + N*	289	263	60
	CH_2N → CH_2* + N*	275	271	9
	CH_3N → CH_3* + N*	213	233	-45
	CNH → C* + NH*	322	295	60
	CHNH → CH* + NH*	243	243	-1
	CH_2NH → CH_2* + NH*	251	274	-51
	CH_3NH → CH_3* + NH*	192	243	-113
	CNH_2 → C* + NH_2*	245	241	8
	$CHNH_2$ → CH* + NH_2*	165	191	-58
	CH_2NH_2 → CH_2* + NH_2*	196	243	-103
	CH_3NH_2 → CH_3* + NH_2*	164	237	-161
Pt(111)	*CN* → C* + N*	386	328	128
	CHN → CH* + N*	293	267	59
	CH_2N → CH_2* + N*	267	268	-2
	CH_3N → CH_3* + N*	215	236	-47
	CNH → C* + NH*	324	297	59

	CHNH → CH* + NH*	228	232	-8
	CH_2NH → CH_2* + NH*	246	272	-57
	CH_3NH → CH_3* + NH*	215	268	-117
	CNH_2 → C* + NH_2*	219	217	3
	$CHNH_2$ → CH* + NH_2*	136	163	-62
	CH_2NH_2 → CH_2* + NH_2*	154	199	-99
	CH_3NH_2 → CH_3* + NH_2*	168	244	-167
Cu(111)	*CN* → C* + N*	553	497	124
	CHN → CH* + N*	418	390	61
	CH_2N → CH_2* + N*	362	360	5
	CH_3N → CH_3* + N*	296	315	-41
	CNH → C* + NH*	439	411	62
	CHNH → CH* + NH*	317	318	-2
	CH_2NH → CH_2* + NH*	266	292	-57
	CH_3NH → CH_3* + NH*	217	265	-107
	CNH_2 → C* + NH_2*	387	384	6
	$CHNH_2$ → CH* + NH_2*	285	303	-40
	CH_2NH_2 → CH_2* + NH_2*	221	270	-110
	CH_3NH_2 → CH_3* + NH_2*	202	271	-154
Ag(111)	*CN* → C* + N*	815	756	131
	CHN → CH* + N*	670	639	68
	CH_2N → CH_2* + N*	576	572	10
	CH_3N → CH_3* + N*	454	469	-34
	CNH → C* + NH*	667	636	70
	CHNH → CH* + NH*	534	531	5
	CH_2NH → CH_2* + NH*	443	468	-55
	CH_3NH → CH_3* + NH*	336	382	-103
	CNH_2 → C* + NH_2*	556	549	16
	$CHNH_2$ → CH* + NH_2*	329	384	-122
	CH_2NH_2 → CH_2* + NH_2*	328	373	-101
	CH_3NH_2 → CH_3* + NH_2*	251	316	-145
Au(111)	*CN* → C* + N*	725	667	128
	CHN → CH* + N*	601	573	61
	CH_2N → CH_2* + N*	545	545	2
	CH_3N → CH_3* + N*	435	451	-37
	CNH → C* + NH*	613	584	64
	CHNH → CH* + NH*	480	482	-5
	CH_2NH → CH_2* + NH*	442	470	-63
	CH_3NH → CH_3* + NH*	359	405	-103
	CNH_2 → C* + NH_2*	507	500	16
	$CHNH_2$ → CH* + NH_2*	395	418	-51
	CH_2NH_2 → CH_2* + NH_2*	328	377	-109
	CH_3NH_2 → CH_3* + NH_2*	265	331	-147

Table S3. DFT-predicted effective barriers (Eqs. 1 and 3) for C–O activation at 450 K and 1 bar H_2

Catalyst	Reaction	$\Delta H^{\neq}$ kJ mol^{-1}	$\Delta G^{\neq}$ kJ mol^{-1}	$\Delta S^{\neq}$ J mol^{-1} K^{-1}
Ru(001)	*CO* → C* + O*	190	167	51
	CHO → CH* + O*	96	102	-14
	CH_2O → CH_2* + O*	125	154	-64
	CH_3O → CH_3* + O*	112	162	-111
	COH → C* + OH*	140	142	-5
	CHOH → CH* + OH*	70	101	-67
	CH_2OH → CH_2* + OH*	80	133	-119
	CH_3OH → CH_3* + OH*	83	169	-191
Os(001)	*CO* → C* + O*	228	205	51
	CHO → CH* + O*	114	122	-17
	CH_2O → CH_2* + O*	147	178	-68
	CH_3O → CH_3* + O*	144	193	-109
	COH → C* + OH*	140	144	-9
	CHOH → CH* + OH*	57	90	-75
	CH_2OH → CH_2* + OH*	67	125	-127
	CH_3OH → CH_3* + OH*	87	175	-196
Co(001)	*CO* → C* + O*	218	185	75
	CHO → CH* + O*	126	121	11
	CH_2O → CH_2* + O*	113	136	-52
	CH_3O → CH_3* + O*	107	148	-91
	COH → C* + OH*	202	191	23
	CHOH → CH* + OH*	119	149	-67
	CH_2OH → CH_2* + OH*	140	179	-87
	CH_3OH → CH_3* + OH*	145	215	-156
Rh(111)	*CO* → C* + O*	236	214	48
	CHO → CH* + O*	147	154	-16
	CH_2O → CH_2* + O*	186	214	-63
	CH_3O → CH_3* + O*	151	202	-115
	COH → C* + OH*	162	165	-6
	CHOH → CH* + OH*	92	124	-72
	CH_2OH → CH_2* + OH*	126	181	-123
	CH_3OH → CH_3* + OH*	119	205	-192
Ir(111)	*CO* → C* + O*	291	270	47
	CHO → CH* + O*	178	187	-19
	CH_2O → CH_2* + O*	168	201	-75
	CH_3O → CH_3* + O*	197	248	-112
	COH → C* + OH*	188	191	-8
	CHOH → CH* + OH*	89	123	-76
	CH_2OH → CH_2* + OH*	109	165	-126
	CH_3OH → CH_3* + OH*	172	246	-164
Ni(111)	*CO* → C* + O*	238	217	46
	CHO → CH* + O*	145	152	-16
	CH_2O → CH_2* + O*	134	168	-74

	CH_3O → CH_3* + O*	119	172	-117
	COH → C* + OH*	206	208	-5
	CHOH → CH* + OH*	125	155	-67
	CH_2OH → CH_2* + OH*	131	184	-117
	CH_3OH → CH_3* + OH*	156	236	-178
Pd(111)	*CO* → C* + O*	327	306	46
	CHO → CH* + O*	237	245	-17
	CH_2O → CH_2* + O*	257	288	-70
	CH_3O → CH_3* + O*	213	265	-114
	COH → C* + OH*	236	238	-4
	CHOH → CH* + OH*	158	189	-70
	CH_2OH → CH_2* + OH*	166	222	-125
	CH_3OH → CH_3* + OH*	187	261	-165
Pt(111)	*CO* → C* + O*	341	321	45
	CHO → CH* + O*	245	254	-19
	CH_2O → CH_2* + O*	260	289	-66
	CH_3O → CH_3* + O*	246	297	-113
	COH → C* + OH*	220	224	-10
	CHOH → CH* + OH*	138	172	-76
	CH_2OH → CH_2* + OH*	172	229	-126
	CH_3OH → CH_3* + OH*	190	264	-164
Cu(111)	*CO* → C* + O*	429	407	49
	CHO → CH* + O*	302	308	-14
	CH_2O → CH_2* + O*	249	279	-66
	CH_3O → CH_3* + O*	195	246	-113
	COH → C* + OH*	379	379	-1
	CHOH → CH* + OH*	258	284	-57
	CH_2OH → CH_2* + OH*	212	263	-113
	CH_3OH → CH_3* + OH*	192	259	-150
Ag(111)	*CO* → C* + O*	644	619	55
	CHO → CH* + O*	505	508	-8
	CH_2O → CH_2* + O*	410	438	-64
	CH_3O → CH_3* + O*	303	351	-106
	COH → C* + OH*	537	533	8
	CHOH → CH* + OH*	391	416	-55
	CH_2OH → CH_2* + OH*	303	352	-108
	CH_3OH → CH_3* + OH*	224	289	-144
Au(111)	*CO* → C* + O*	605	582	49
	CHO → CH* + O*	479	487	-18
	CH_2O → CH_2* + O*	435	467	-72
	CH_3O → CH_3* + O*	342	390	-107
	COH → C* + OH*	486	483	7
	CHOH → CH* + OH*	372	402	-65
	CH_2OH → CH_2* + OH*	311	366	-122
	CH_3OH → CH_3* + OH*	254	324	-156

Table S4. DFT-predicted effective barriers (Eqs. 1 and 3) for C–S activation at 450 K and 1 bar H_2

Catalyst	Reaction	$\Delta H^{\neq}$ kJ mol^{-1}	$\Delta G^{\neq}$ kJ mol^{-1}	$\Delta S^{\neq}$ J mol^{-1} K^{-1}
Ru(001)	*CS* → C* + S*	-6	-29	50
	CHS → CH* + S*	-73	-68	-11
	CH_2S → CH_2* + S*	-71	-41	-65
	CH_3S → CH_3* + S*	-67	-17	-113
	CSH → C* + SH*	80	80	0
	CHSH → CH* + SH*	24	55	-69
	CH_2SH → CH_2* + SH*	33	83	-111
	CH_3SH → CH_3* + SH*	43	117	-164
Os(001)	*CS* → C* + S*	29	6	51
	CHS → CH* + S*	-56	-49	-15
	CH_2S → CH_2* + S*	-51	-19	-70
	CH_3S → CH_3* + S*	-47	5	-115
	CSH → C* + SH*	92	93	-2
	CHSH → CH* + SH*	31	59	-63
	CH_2SH → CH_2* + SH*	31	83	-117
	CH_3SH → CH_3* + SH*	68	143	-166
Co(001)	*CS* → C* + S*	57	24	73
	CHS → CH* + S*	-20	-16	-10
	CH_2S → CH_2* + S*	-29	-10	-41
	CH_3S → CH_3* + S*	-26	14	-88
	CSH → C* + SH*	136	122	32
	CHSH → CH* + SH*	40	68	-62
	CH_2SH → CH_2* + SH*	47	89	-94
	CH_3SH → CH_3* + SH*	11	89	-172
Rh(111)	*CS* → C* + S*	45	19	58
	CHS → CH* + S*	-43	-38	-12
	CH_2S → CH_2* + S*	-33	-2	-69
	CH_3S → CH_3* + S*	-55	-4	-112
	CSH → C* + SH*	89	90	-3
	CHSH → CH* + SH*	28	55	-61
	CH_2SH → CH_2* + SH*	45	96	-114
	CH_3SH → CH_3* + SH*	56	136	-179
Ir(111)	*CS* → C* + S*	93	68	54
	CHS → CH* + S*	-10	-3	-16
	CH_2S → CH_2* + S*	3	35	-72
	CH_3S → CH_3* + S*	-16	35	-115
	CSH → C* + SH*	119	120	-3
	CHSH → CH* + SH*	44	73	-65
	CH_2SH → CH_2* + SH*	80	135	-121
	CH_3SH → CH_3* + SH*	83	167	-186
Ni(111)	*CS* → C* + S*	52	31	46
	CHS → CH* + S*	-23	-18	-13
	CH_2S → CH_2* + S*	-30	1	-67

	CH_3S → CH_3* + S*	-33	18	-112
	CSH → C* + SH*	171	173	-4
	CHSH → CH* + SH*	70	99	-64
	CH_2SH → CH_2* + SH*	49	100	-114
	CH_3SH → CH_3* + SH*	62	137	-169
Pd(111)	*CS* → C* + S*	103	82	46
	CHS → CH* + S*	34	40	-13
	CH_2S → CH_2* + S*	36	68	-69
	CH_3S → CH_3* + S*	-6	44	-111
	CSH → C* + SH*	157	158	-2
	CHSH → CH* + SH*	100	129	-64
	CH_2SH → CH_2* + SH*	81	134	-118
	CH_3SH → CH_3* + SH*	56	132	-170
Pt(111)	*CS* → C* + S*	116	96	44
	CHS → CH* + S*	44	51	-15
	CH_2S → CH_2* + S*	49	83	-74
	CH_3S → CH_3* + S*	8	58	-112
	CSH → C* + SH*	142	143	-4
	CHSH → CH* + SH*	72	101	-66
	CH_2SH → CH_2* + SH*	93	148	-121
	CH_3SH → CH_3* + SH*	78	157	-177
Cu(111)	*CS* → C* + S*	275	253	50
	CHS → CH* + S*	152	157	-10
	CH_2S → CH_2* + S*	93	123	-67
	CH_3S → CH_3* + S*	62	110	-107
	CSH → C* + SH*	313	313	1
	CHSH → CH* + SH*	203	230	-58
	CH_2SH → CH_2* + SH*	146	196	-112
	CH_3SH → CH_3* + SH*	142	210	-152
Ag(111)	*CS* → C* + S*	478	452	57
	CHS → CH* + S*	292	321	-65
	CH_2S → CH_2* + S*	239	267	-62
	CH_3S → CH_3* + S*	151	197	-100
	CSH → C* + SH*	475	471	10
	CHSH → CH* + SH*	346	369	-51
	CH_2SH → CH_2* + SH*	245	292	-107
	CH_3SH → CH_3* + SH*	183	247	-142
Au(111)	*CS* → C* + S*	410	387	51
	CHS → CH* + S*	314	320	-11
	CH_2S → CH_2* + S*	242	274	-71
	CH_3S → CH_3* + S*	162	209	-104
	CSH → C* + SH*	426	422	7
	CHSH → CH* + SH*	321	348	-60
	CH_2SH → CH_2* + SH*	235	287	-117
	CH_3SH → CH_3* + SH*	186	257	-156

Table S5. DFT-predicted effective barriers (Eqs. 1 and 3) for C–Cl activation at 450 K and 1 bar H_2

Catalyst	Reaction	$\Delta H^{\ddagger}$ kJ mol^{-1}	$\Delta G^{\ddagger}$ kJ mol^{-1}	$\Delta S^{\ddagger}$ J mol^{-1} K^{-1}
Ru(001)	*CCl* → C* + Cl*	54	54	1
	CHCl → CH* + Cl*	39	65	-58
	CH_2Cl → CH_2* + Cl*	35	85	-111
	CH_3Cl → CH_3* + Cl*	72	132	-135
Os(001)	*CCl* → C* + Cl*	66	68	-3
	CHCl → CH* + Cl*	44	70	-58
	CH_2Cl → CH_2* + Cl*	35	87	-116
	CH_3Cl → CH_3* + Cl*	119	180	-137
Co(001)	*CCl* → C* + Cl*	125	122	5
	CHCl → CH* + Cl*	88	111	-52
	CH_2Cl → CH_2* + Cl*	90	125	-79
	CH_3Cl → CH_3* + Cl*	71	121	-111
Rh(111)	*CCl* → C* + Cl*	132	128	8
	CHCl → CH* + Cl*	56	82	-58
	CH_2Cl → CH_2* + Cl*	44	93	-111
	CH_3Cl → CH_3* + Cl*	119	182	-140
Ir(111)	*CCl* → C* + Cl*	185	182	7
	CHCl → CH* + Cl*	68	97	-63
	CH_2Cl → CH_2* + Cl*	52	106	-120
	CH_3Cl → CH_3* + Cl*	144	206	-138
Ni(111)	*CCl* → C* + Cl*	150	148	5
	CHCl → CH* + Cl*	95	118	-52
	CH_2Cl → CH_2* + Cl*	94	138	-98
	CH_3Cl → CH_3* + Cl*	83	142	-132
Pd(111)	*CCl* → C* + Cl*	161	159	4
	CHCl → CH* + Cl*	109	132	-52
	CH_2Cl → CH_2* + Cl*	117	164	-103
	CH_3Cl → CH_3* + Cl*	138	201	-139
Pt(111)	*CCl* → C* + Cl*	185	184	3
	CHCl → CH* + Cl*	102	129	-60
	CH_2Cl → CH_2* + Cl*	98	144	-103
	CH_3Cl → CH_3* + Cl*	153	216	-142
Cu(111)	*CCl* → C* + Cl*	310	307	8
	CHCl → CH* + Cl*	209	229	-46
	CH_2Cl → CH_2* + Cl*	154	199	-102
	CH_3Cl → CH_3* + Cl*	146	203	-125
Ag(111)	*CCl* → C* + Cl*	453	448	13
	CHCl → CH* + Cl*	325	344	-42
	CH_2Cl → CH_2* + Cl*	228	272	-96
	CH_3Cl → CH_3* + Cl*	165	222	-125
Au(111)	*CCl* → C* + Cl*	397	394	6
	CHCl → CH* + Cl*	314	335	-47
	CH_2Cl → CH_2* + Cl*	252	299	-103

$*CH_3Cl* \rightarrow CH_3* + Cl*$	204	265	-136

S4. Transition State Structures

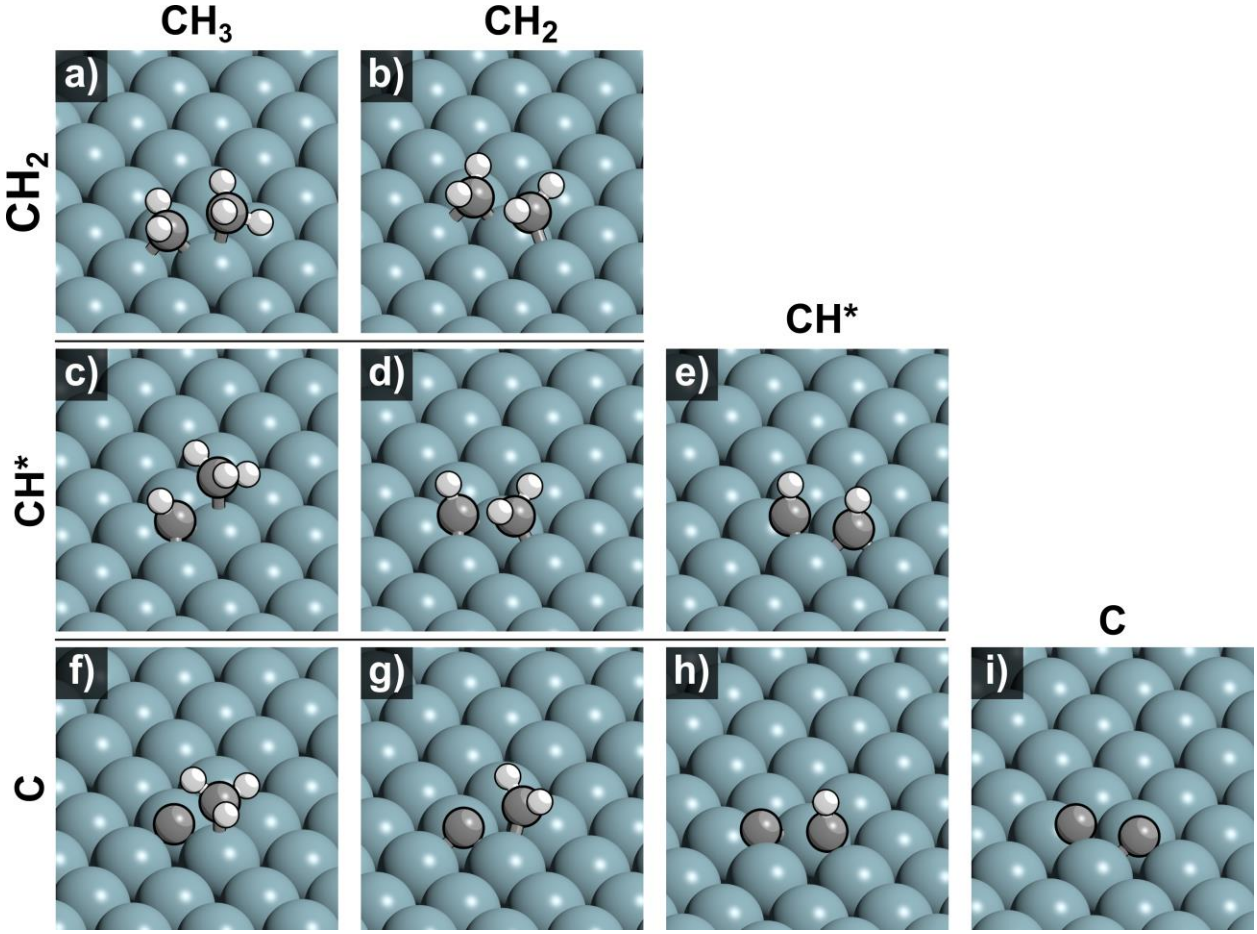

Figure S7. Transition state structures for C–C bond cleavage in ethane-derived intermediates on Ru(001) surface. Calculated $\Delta H^{\ddagger}$ and $\Delta G^{\ddagger}$ values are shown in Table S1. Structures and their reaction mode files (POSCAR and MODECAR files) are available in the supporting information.

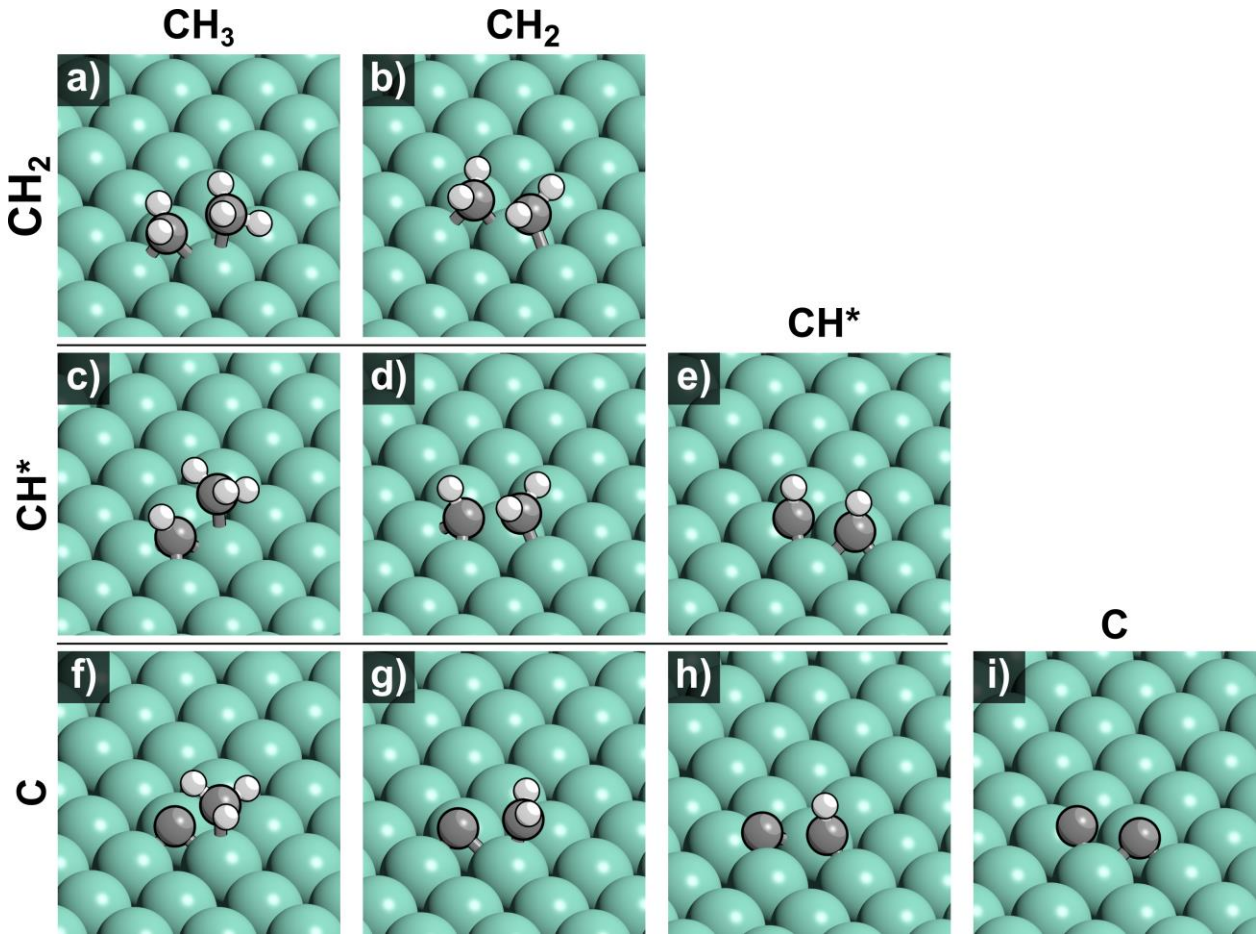

Figure S8. Transition state structures for C–C bond cleavage in ethane-derived intermediates on Os(001) surface. Calculated $\Delta H^{\ddagger}$ and $\Delta G^{\ddagger}$ values are shown in Table S1. Structures and their reaction mode files (POSCAR and MODECAR files) are available in the supporting information.

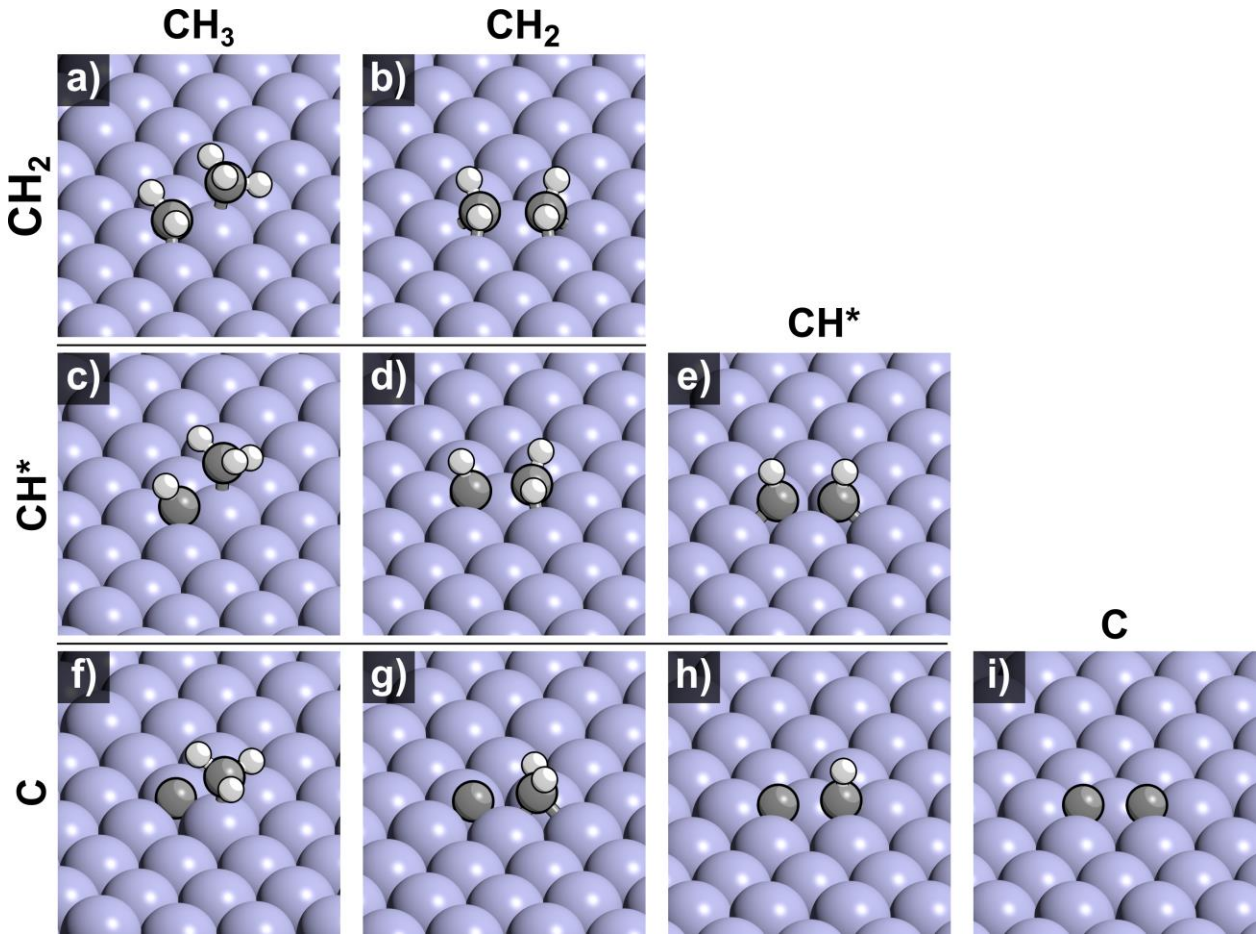

Figure S9. Transition state structures for C–C bond cleavage in ethane-derived intermediates on Co(001) surface. Calculated $\Delta H^{\ddagger}$ and $\Delta G^{\ddagger}$ values are shown in Table S1. Structures and their reaction mode files (POSCAR and MODECAR files) are available in the supporting information.

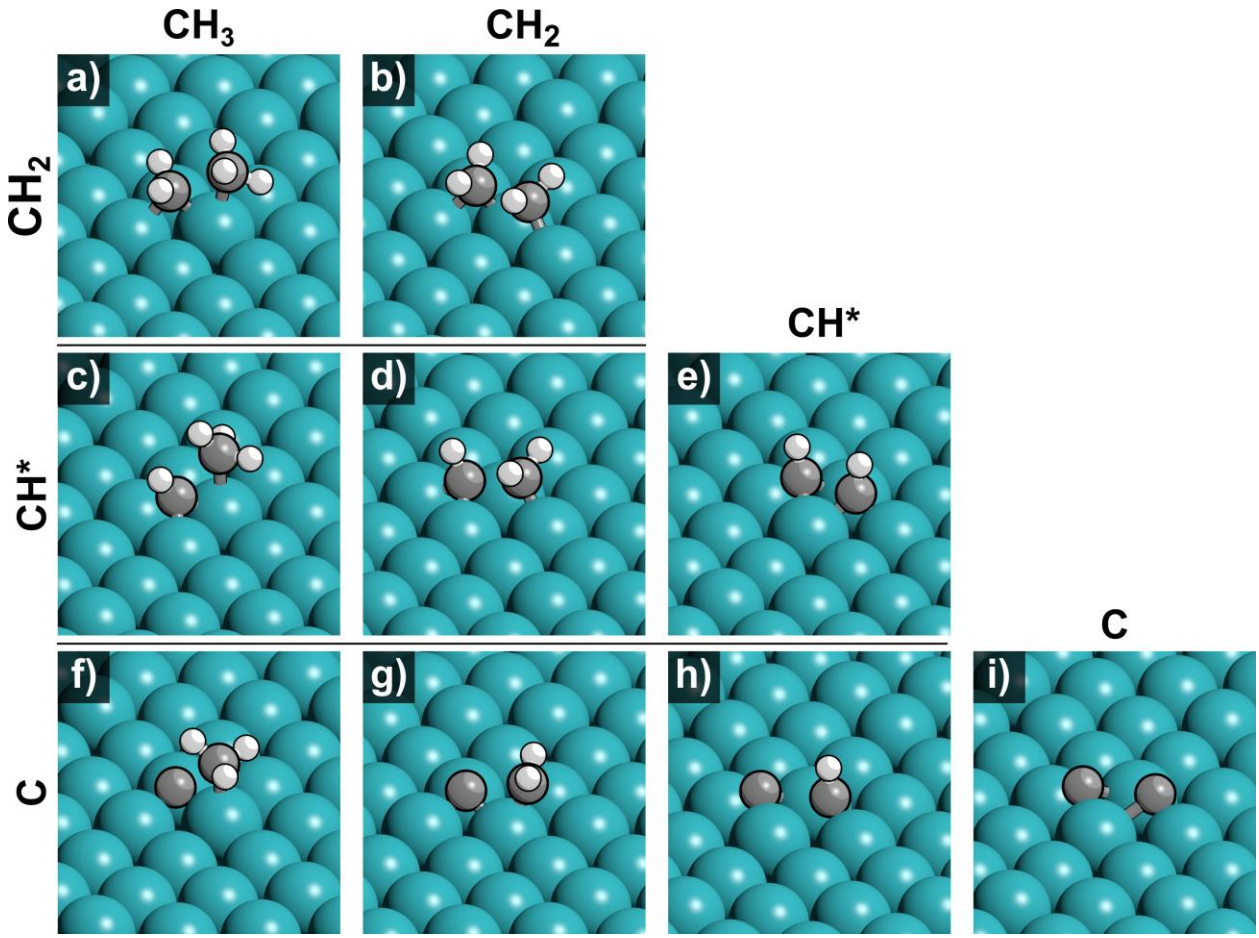

Figure S10. Transition state structures for C–C bond cleavage in ethane-derived intermediates on Rh(111) surface. Calculated $\Delta H^{\ddagger}$ and $\Delta G^{\ddagger}$ values are shown in Table S1. Structures and their reaction mode files (POSCAR and MODECAR files) are available in the supporting information.

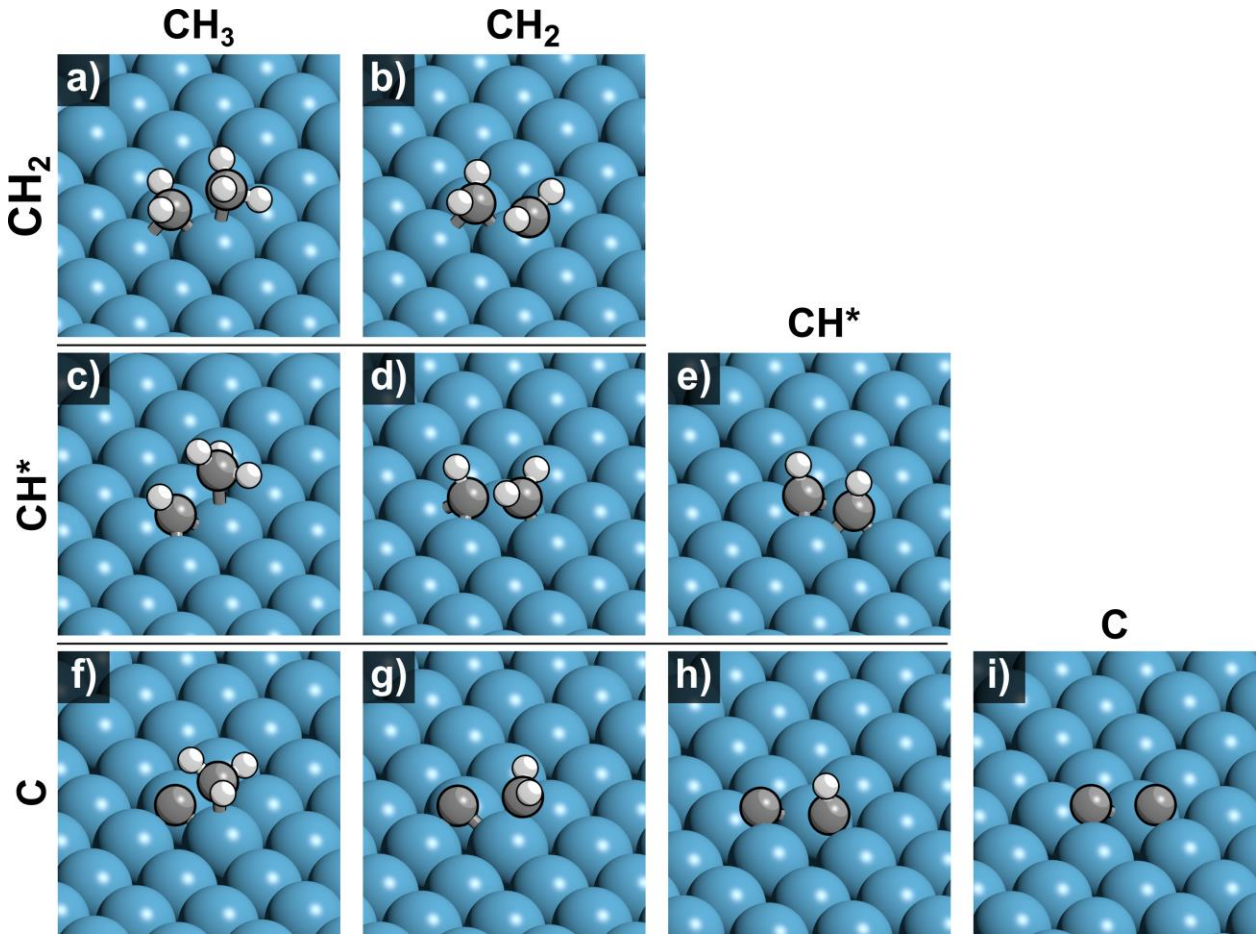

Figure S11. Transition state structures for C–C bond cleavage in ethane-derived intermediates on Ir(111) surface. Calculated $\Delta H^{\ddagger}$ and $\Delta G^{\ddagger}$ values are shown in Table S1. Structures and their reaction mode files (POSCAR and MODECAR files) are available in the supporting information.

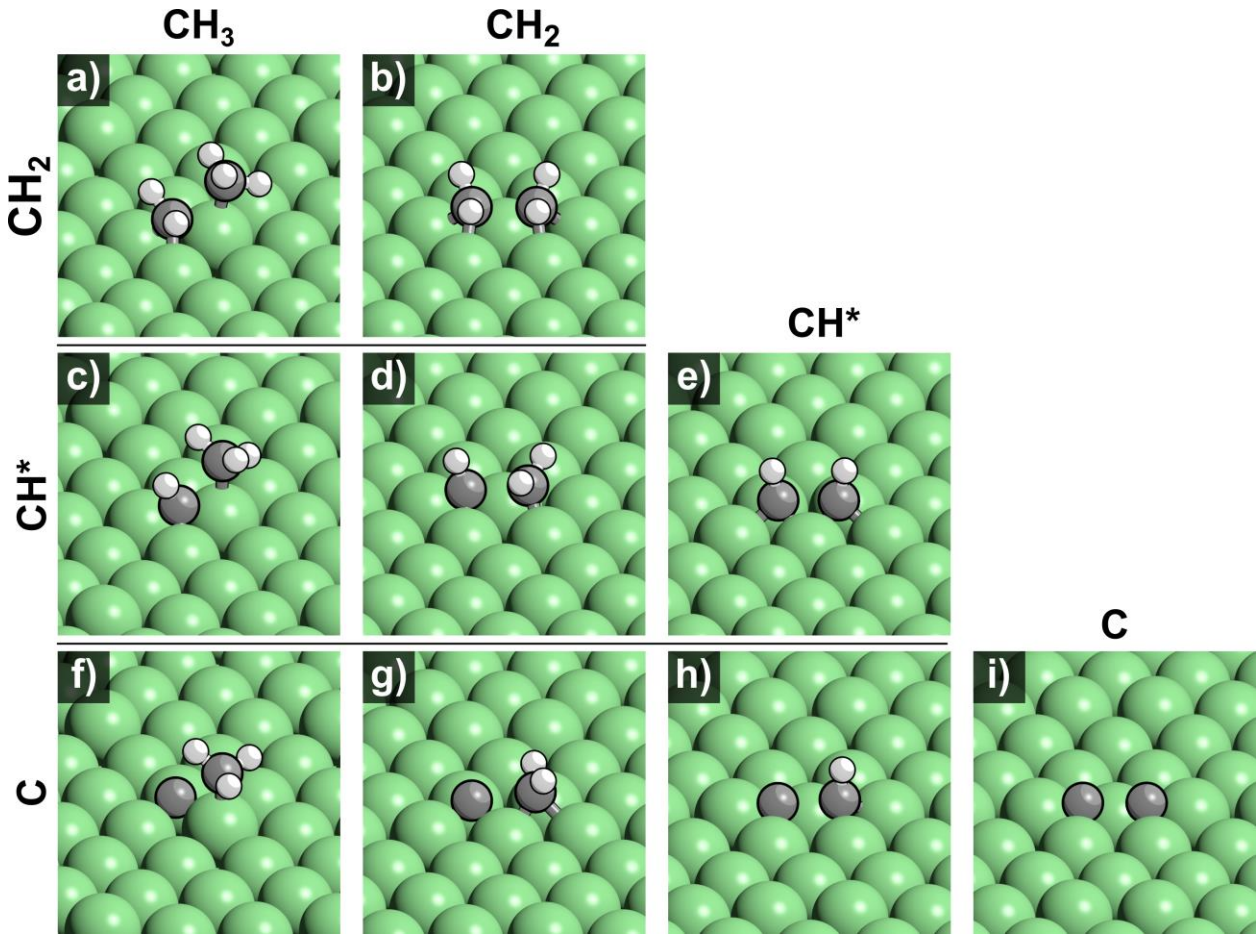

Figure S12. Transition state structures for C–C bond cleavage in ethane-derived intermediates on Ni(111) surface. Calculated $\Delta H^{\ddagger}$ and $\Delta G^{\ddagger}$ values are shown in Table S1. Structures and their reaction mode files (POSCAR and MODECAR files) are available in the supporting information.

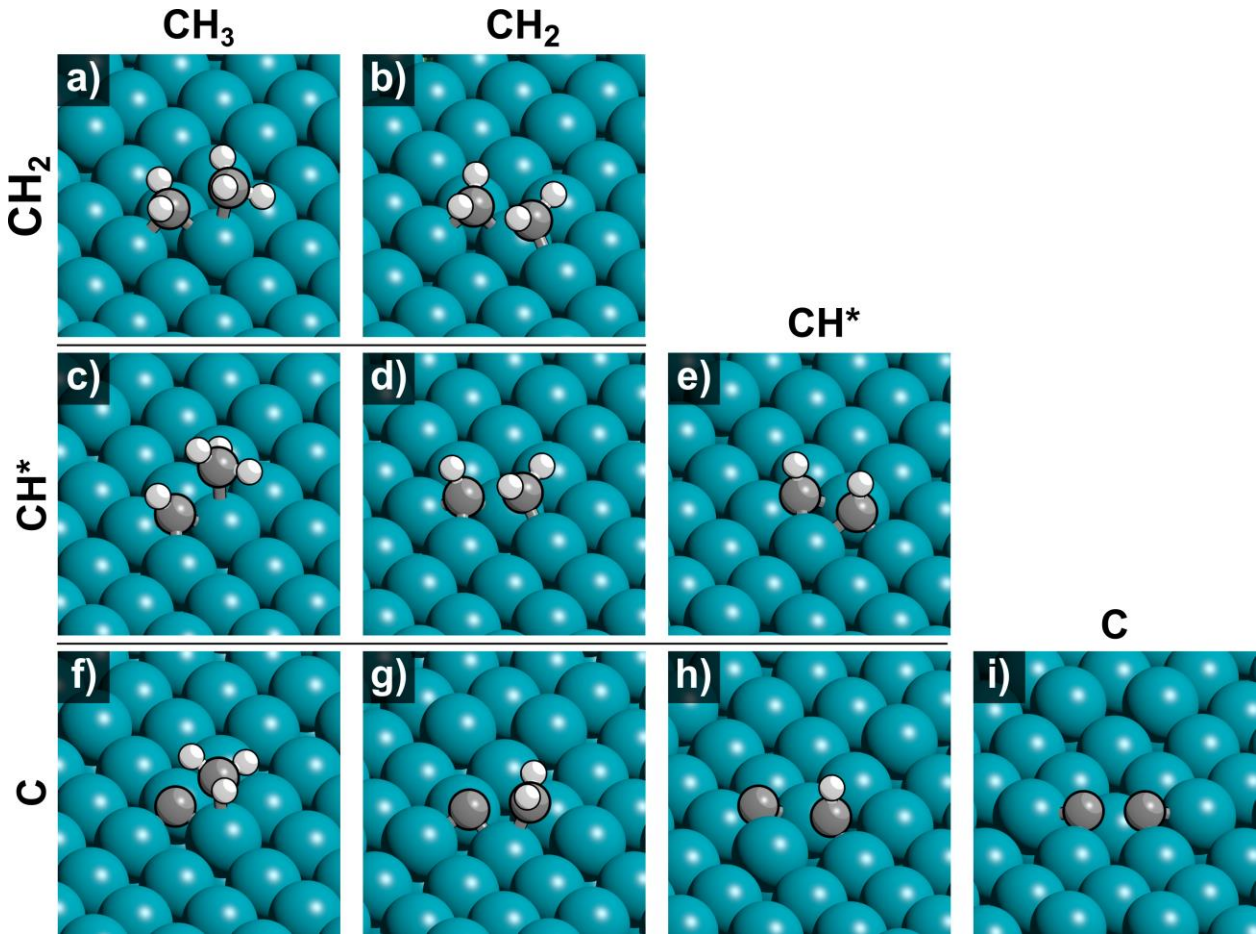

Figure S13. Transition state structures for C–C bond cleavage in ethane-derived intermediates on Pd(111) surface. Calculated $\Delta H^{\ddagger}$ and $\Delta G^{\ddagger}$ values are shown in Table S1. Structures and their reaction mode files (POSCAR and MODECAR files) are available in the supporting information.

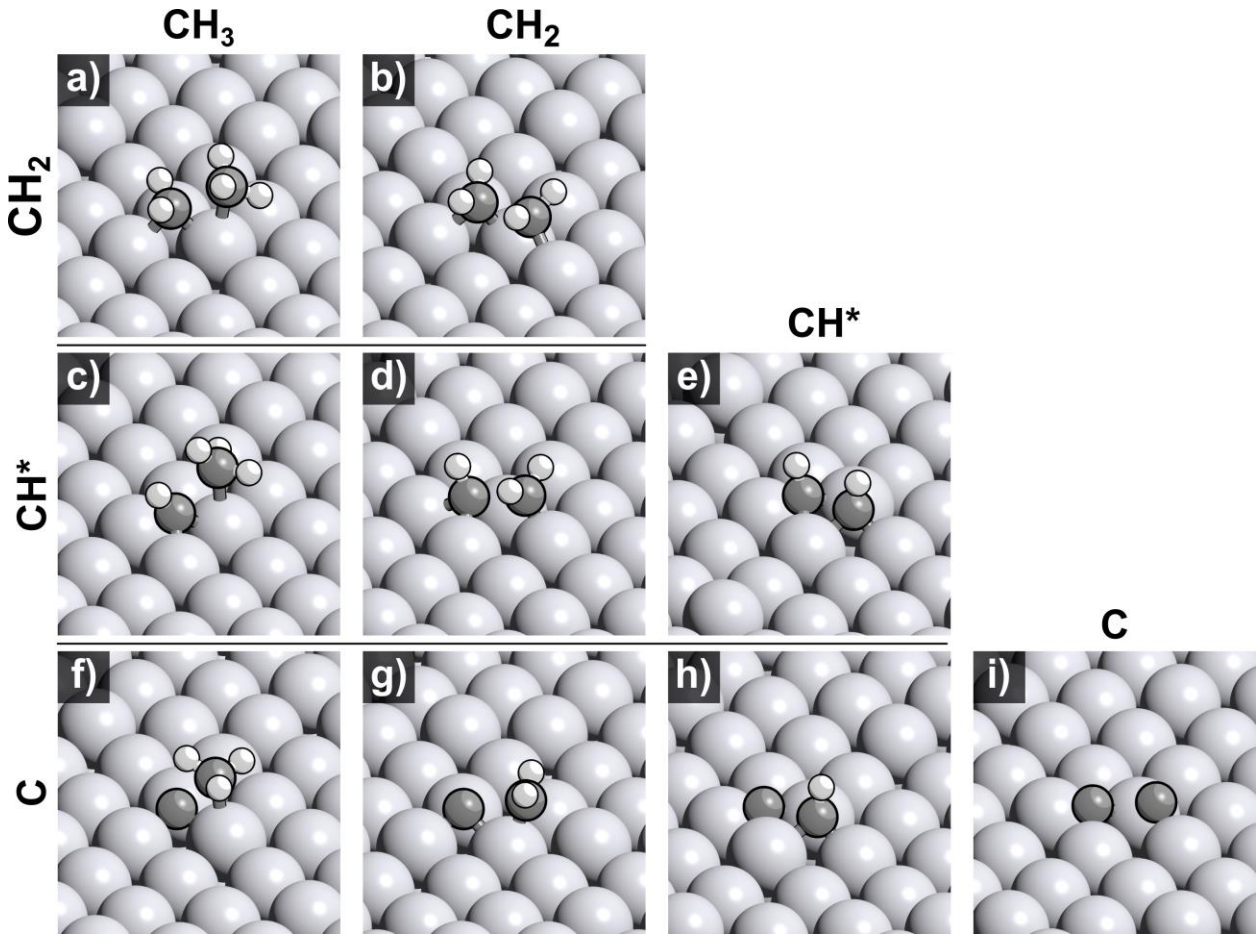

Figure S14. Transition state structures for C–C bond cleavage in ethane-derived intermediates on Pt(111) surface. Calculated $\Delta H^{\ddagger}$ and $\Delta G^{\ddagger}$ values are shown in Table S1. Structures and their reaction mode files (POSCAR and MODECAR files) are available in the supporting information.

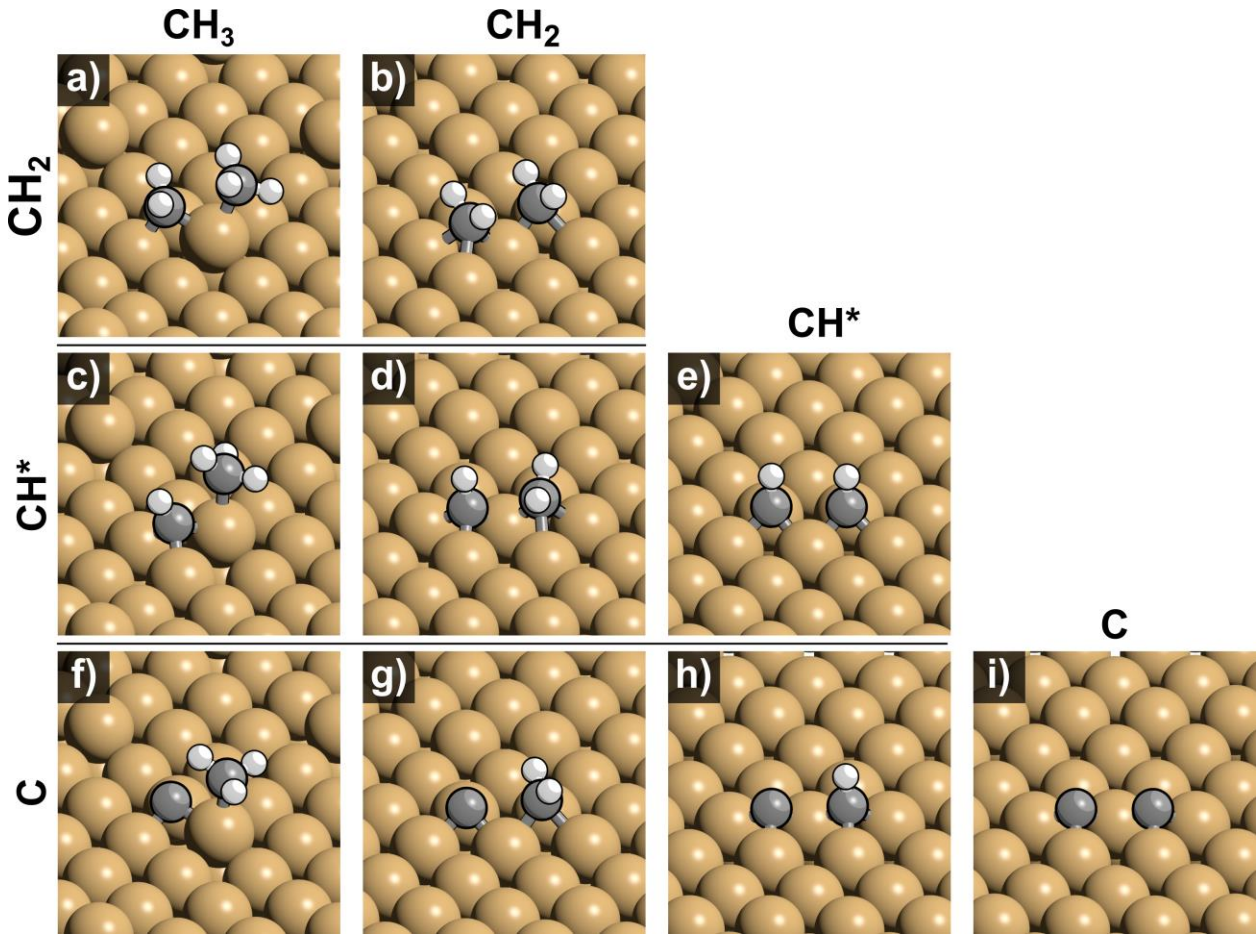

Figure S15. Transition state structures for C–C bond cleavage in ethane-derived intermediates on Cu(111) surface. Calculated $\Delta H^{\ddagger}$ and $\Delta G^{\ddagger}$ values are shown in Table S1. Structures and their reaction mode files (POSCAR and MODECAR files) are available in the supporting information.

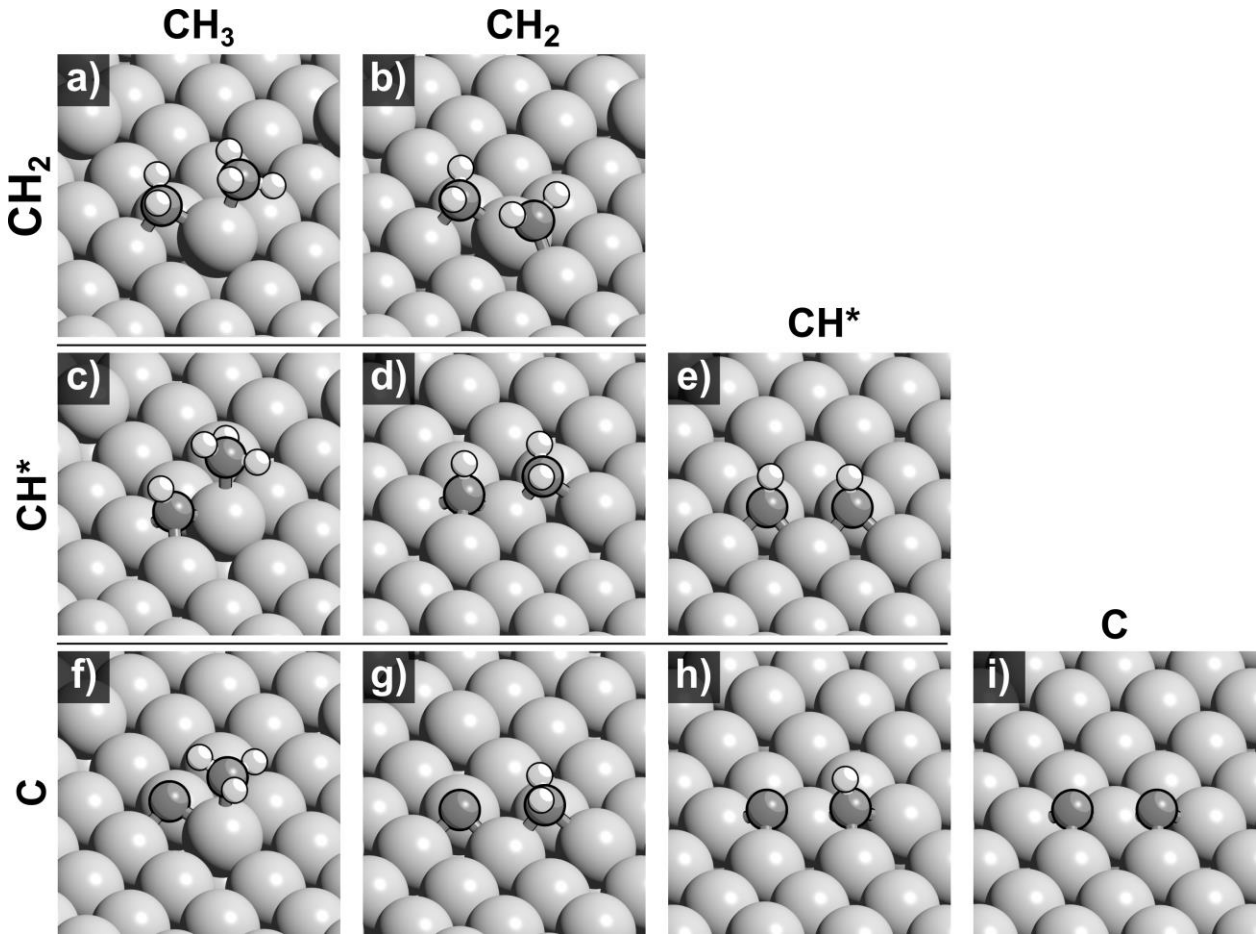

Figure S16. Transition state structures for C–C bond cleavage in ethane-derived intermediates on Ag(111) surface. Calculated $\Delta H^{\ddagger}$ and $\Delta G^{\ddagger}$ values are shown in Table S1. Structures and their reaction mode files (POSCAR and MODECAR files) are available in the supporting information.

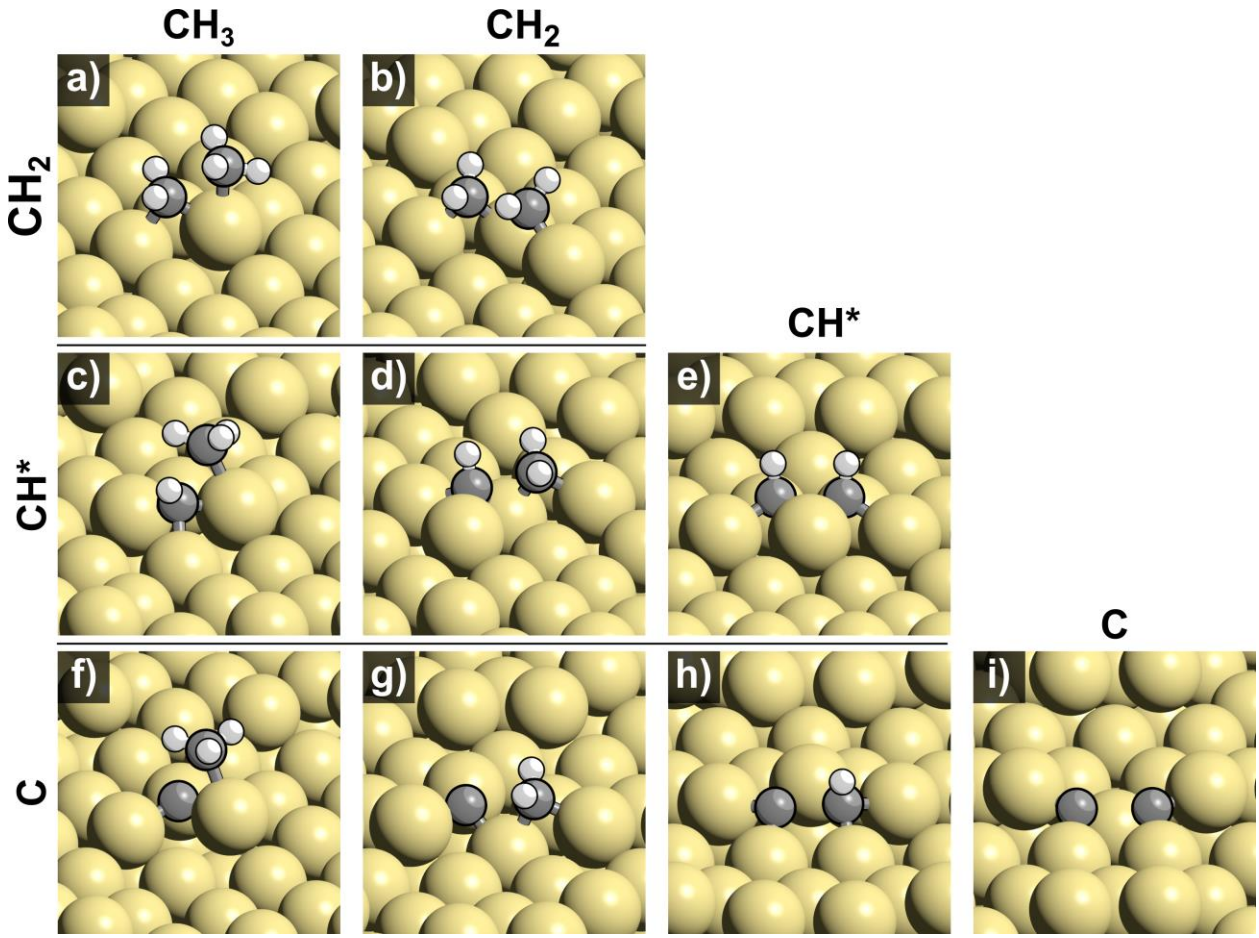

Figure S17. Transition state structures for C–C bond cleavage in ethane-derived intermediates on Au(111) surface. Calculated $\Delta H^{\ddagger}$ and $\Delta G^{\ddagger}$ values are shown in Table S1. Structures and their reaction mode files (POSCAR and MODECAR files) are available in the supporting information.

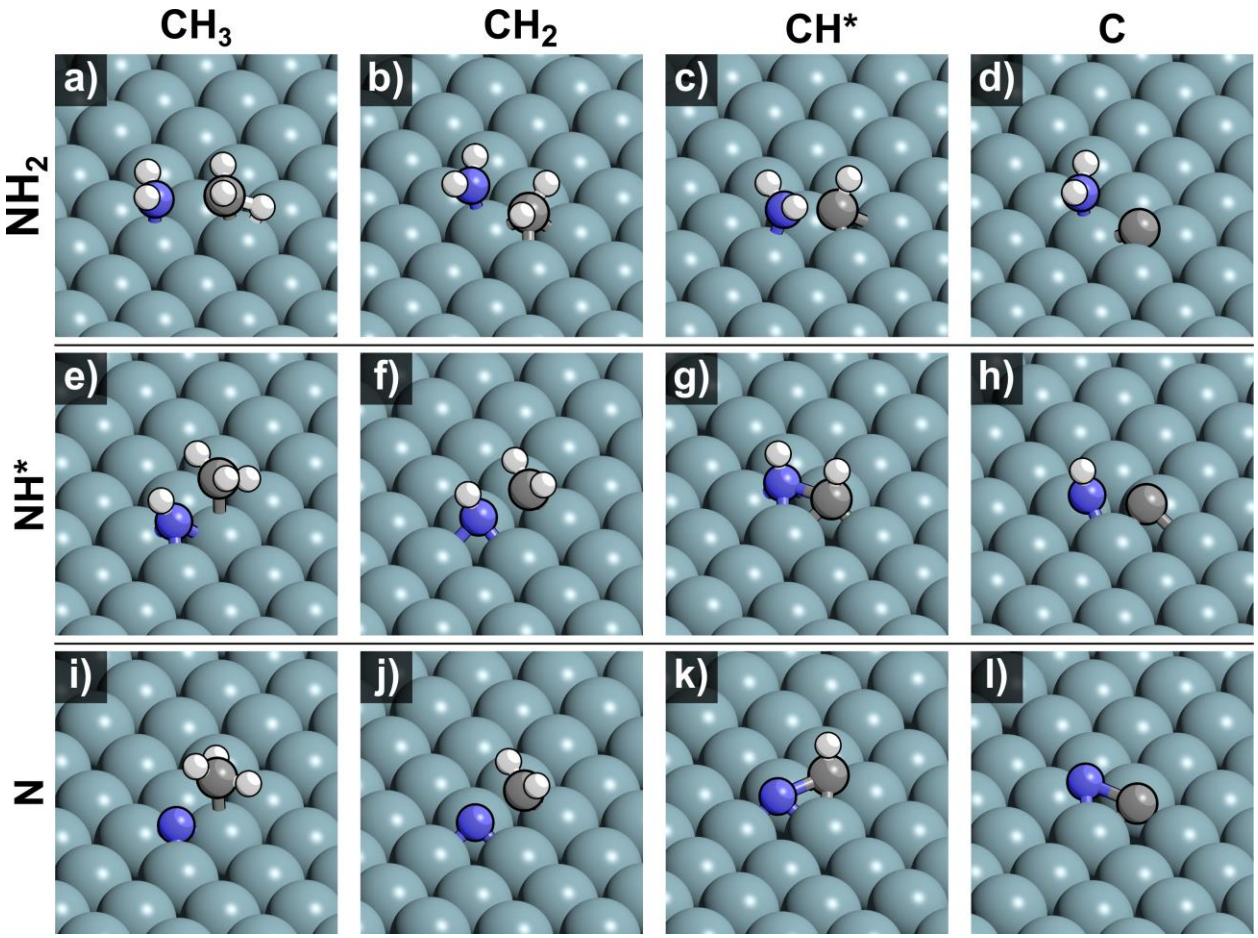

Figure S18. Transition state structures for C–N bond cleavage in methylamine-derived intermediates on Ru(001) surface. Calculated $\Delta H^{\neq}$ and $\Delta G^{\neq}$ values are shown in Table S2. Structures and their reaction mode files (POSCAR and MODECAR files) are available in the supporting information.

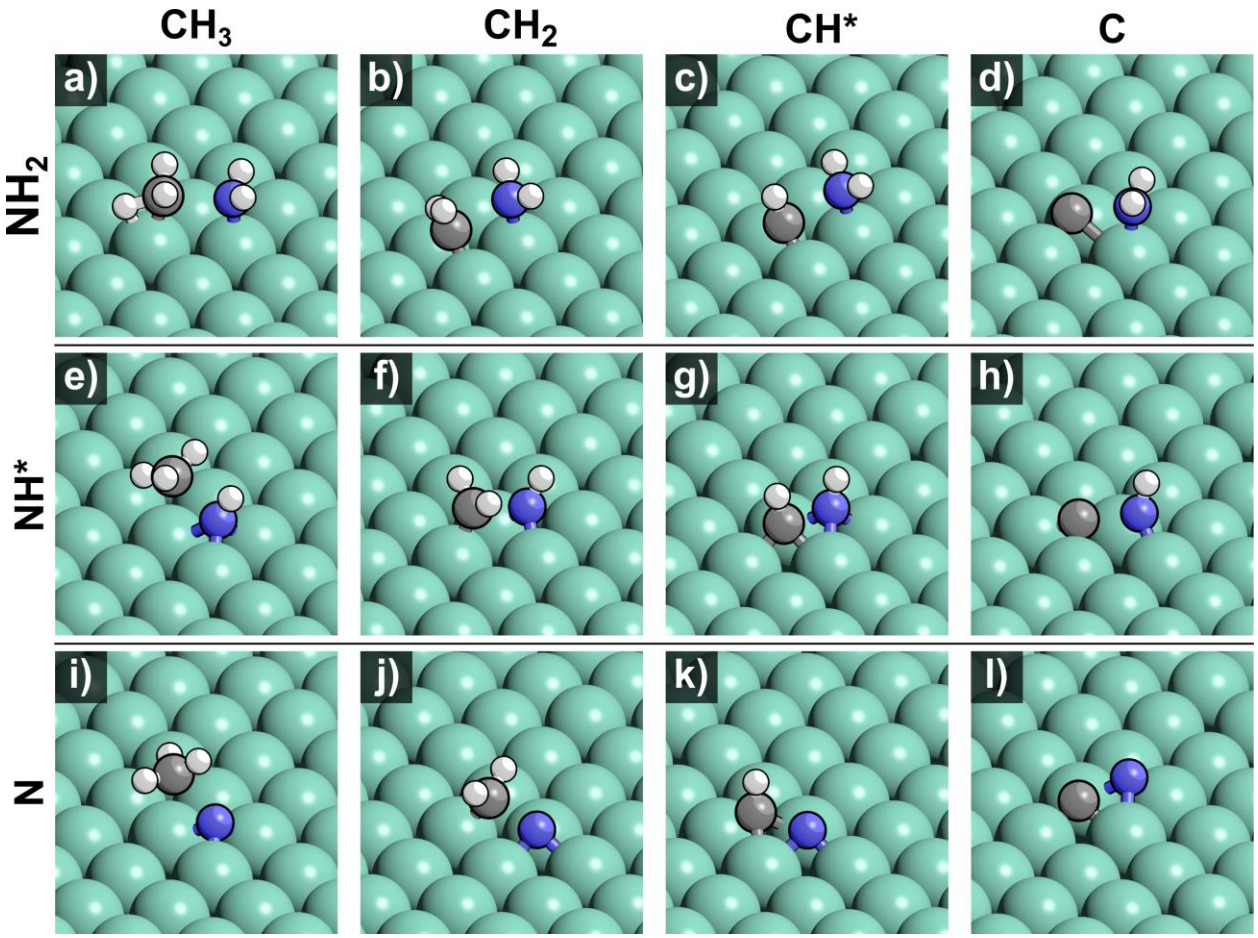

Figure S19. Transition state structures for C–N bond cleavage in methylamine-derived intermediates on Os(001) surface. Calculated $\Delta H^{\neq}$ and $\Delta G^{\neq}$ values are shown in Table S2. Structures and their reaction mode files (POSCAR and MODECAR files) are available in the supporting information.

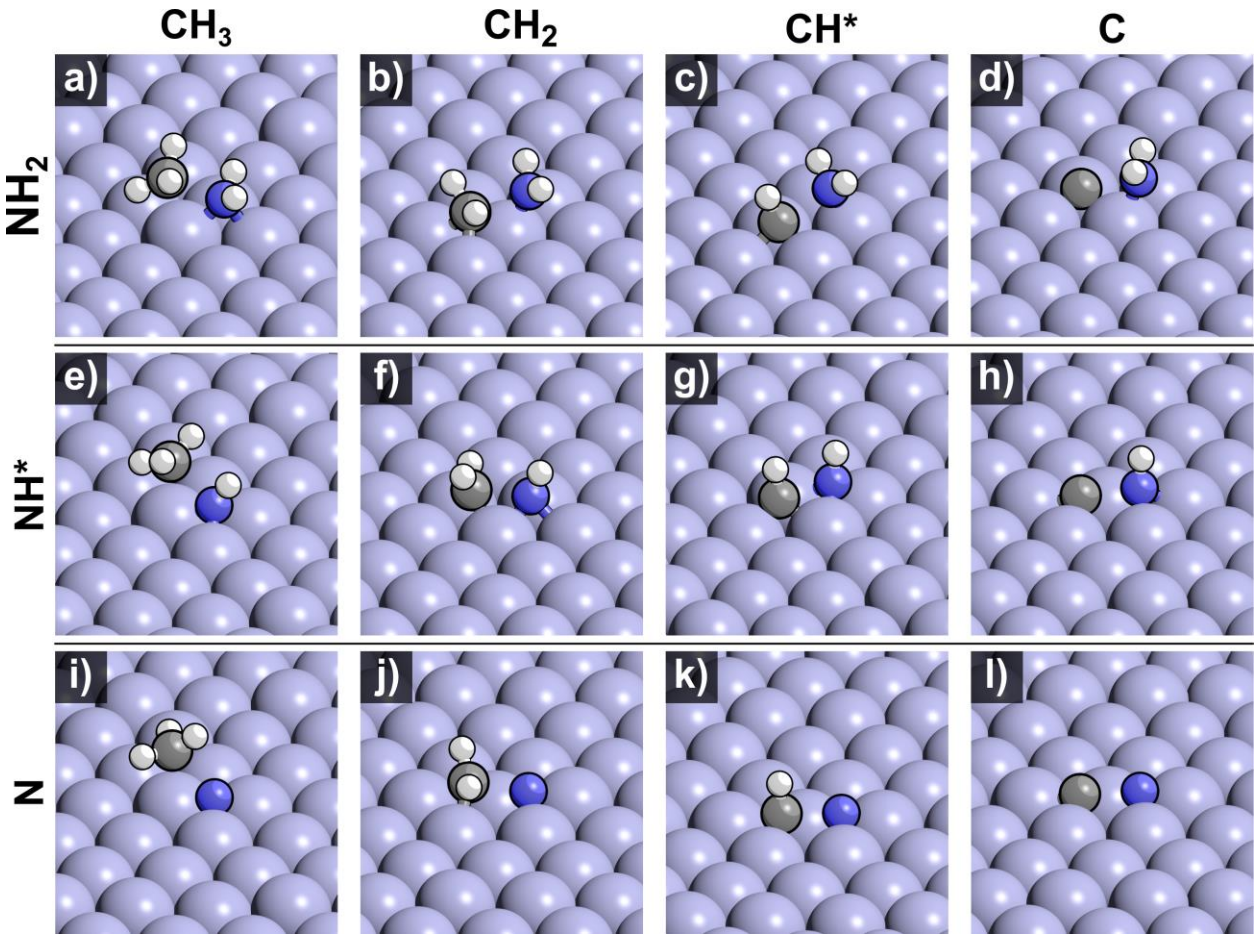

Figure S20. Transition state structures for C–N bond cleavage in methylamine-derived intermediates on Co(001) surface. Calculated $\Delta H^{\neq}$ and $\Delta G^{\neq}$ values are shown in Table S2. Structures and their reaction mode files (POSCAR and MODECAR files) are available in the supporting information.

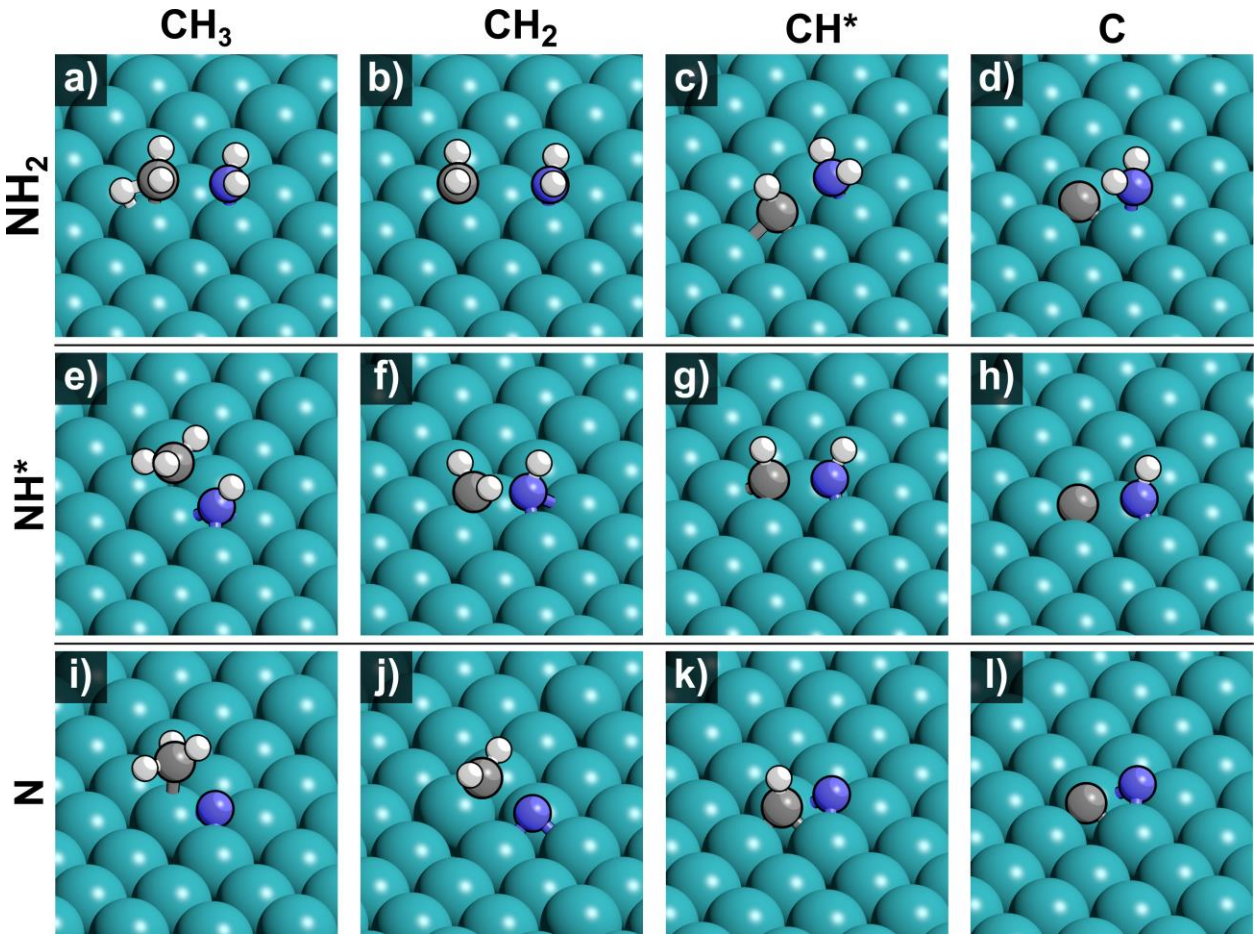

Figure S21. Transition state structures for C–N bond cleavage in methylamine-derived intermediates on Rh(111) surface. Calculated $\Delta H^{\neq}$ and $\Delta G^{\neq}$ values are shown in Table S2. Structures and their reaction mode files (POSCAR and MODECAR files) are available in the supporting information.

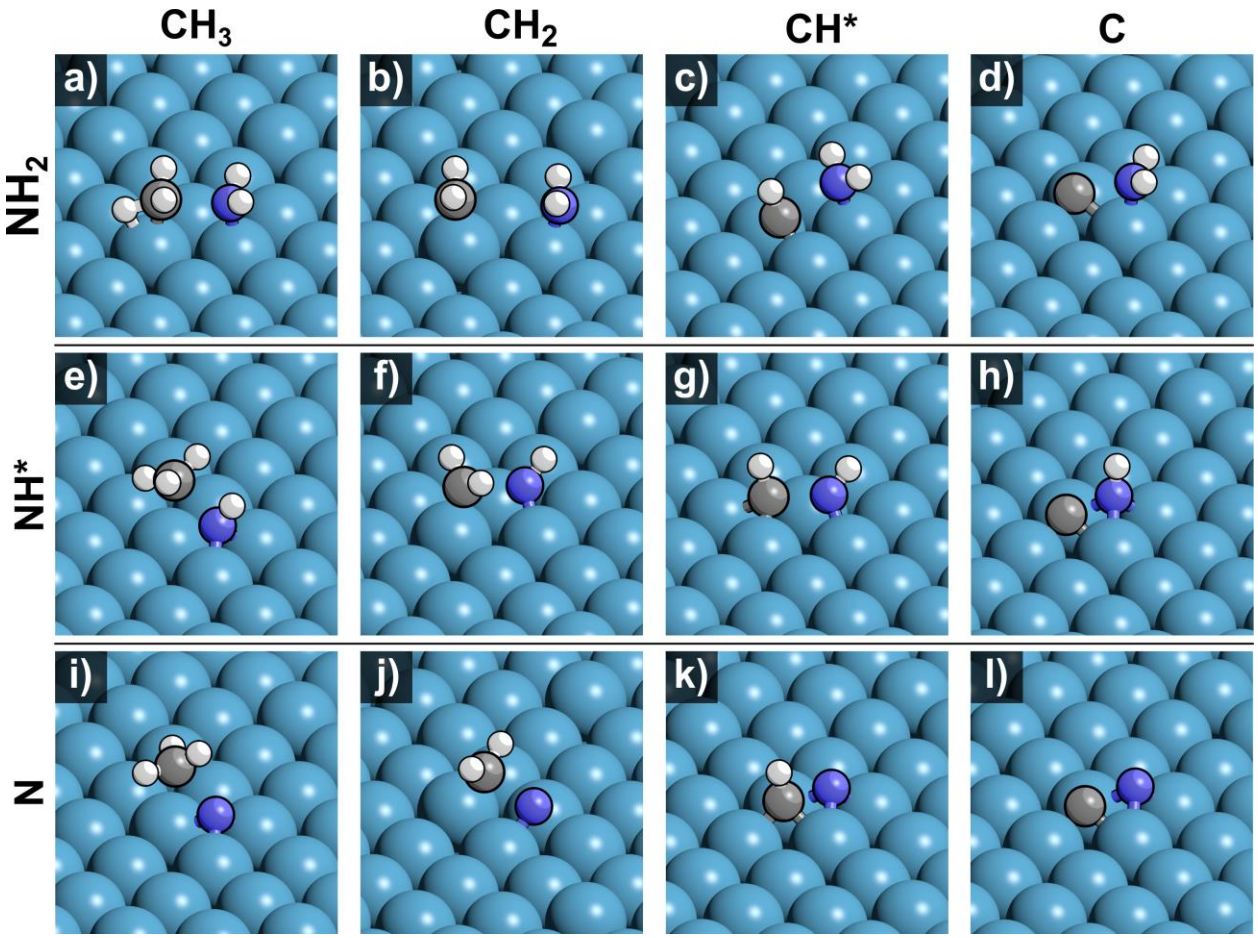

Figure S22. Transition state structures for C–N bond cleavage in methylamine-derived intermediates on Ir(111) surface. Calculated $\Delta H^{\ddagger}$ and $\Delta G^{\ddagger}$ values are shown in Table S2. Structures and their reaction mode files (POSCAR and MODECAR files) are available in the supporting information.

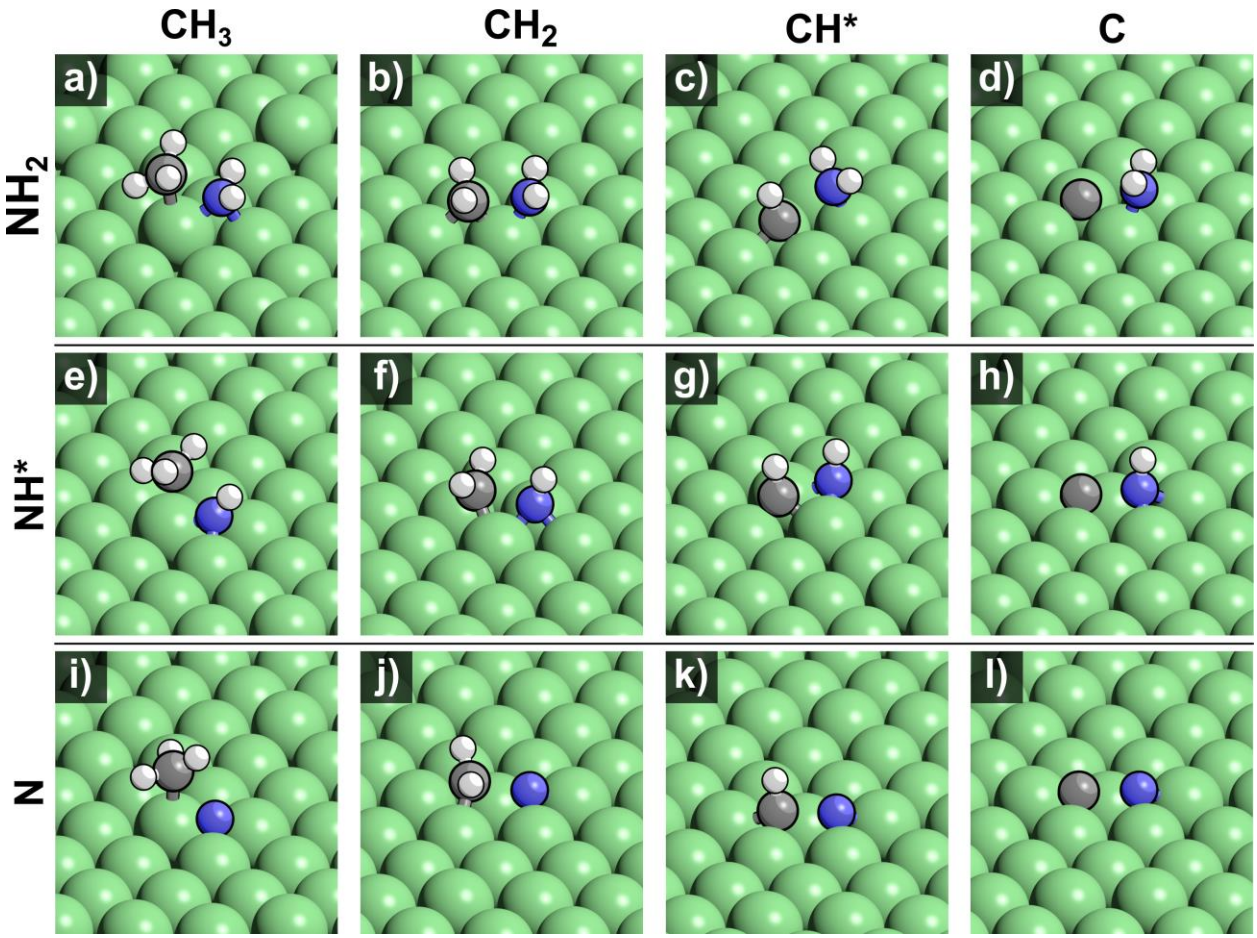

Figure S23. Transition state structures for C–N bond cleavage in methylamine-derived intermediates on Ni(111) surface. Calculated $\Delta H^{\neq}$ and $\Delta G^{\neq}$ values are shown in Table S2. Structures and their reaction mode files (POSCAR and MODECAR files) are available in the supporting information.

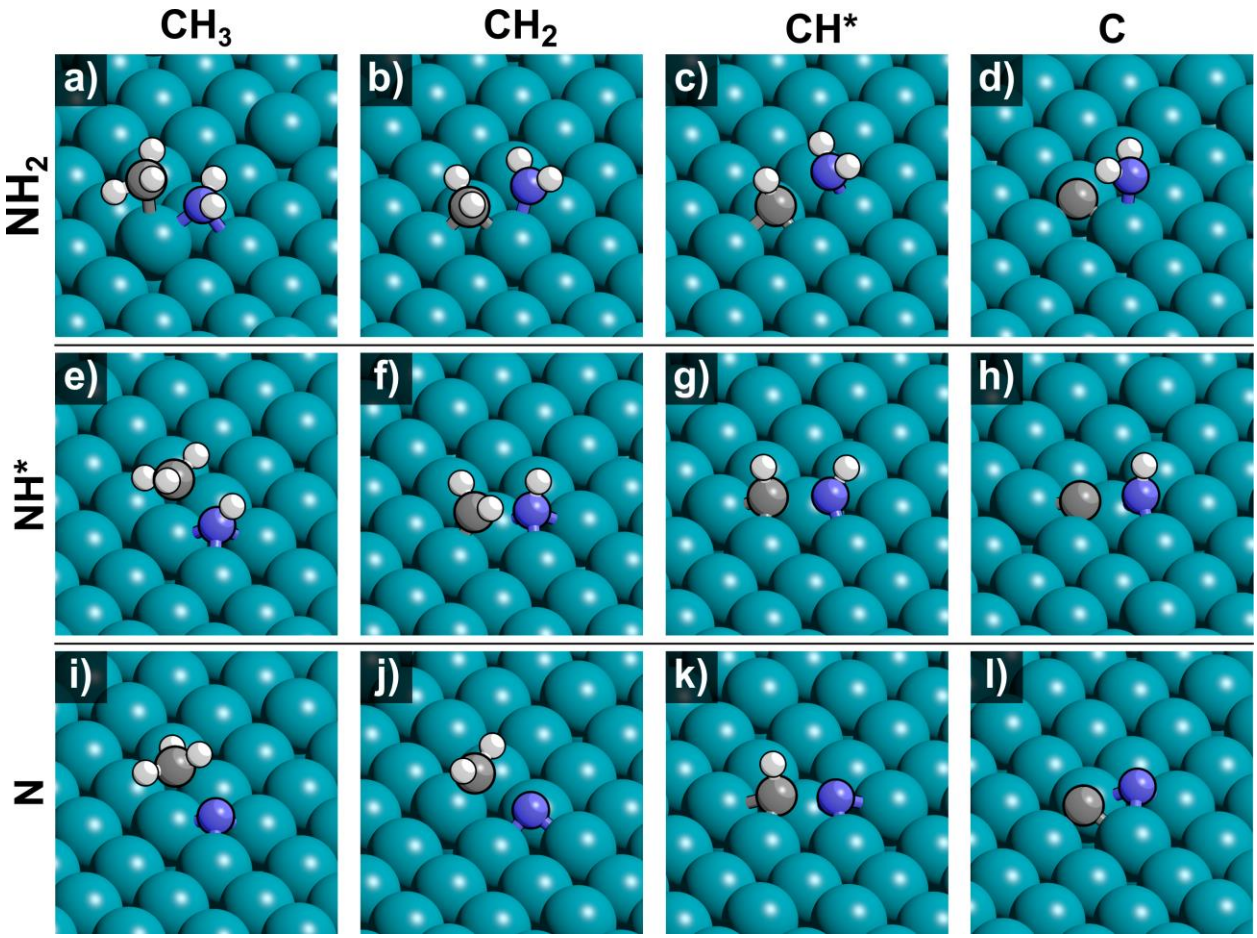

Figure S24. Transition state structures for C–N bond cleavage in methylamine-derived intermediates on Pd(111) surface. Calculated $\Delta H^{\neq}$ and $\Delta G^{\neq}$ values are shown in Table S2. Structures and their reaction mode files (POSCAR and MODECAR files) are available in the supporting information.

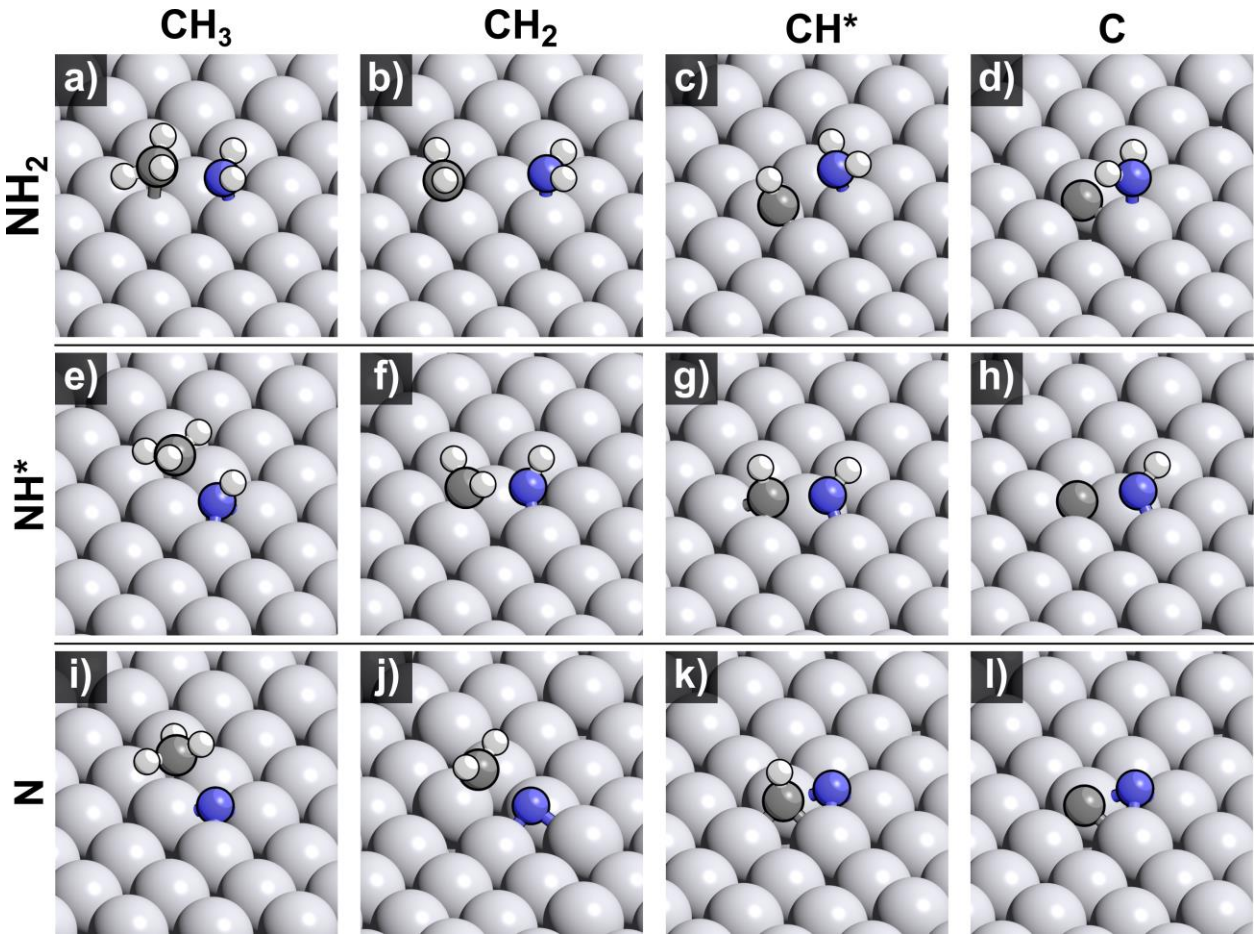

Figure S25. Transition state structures for C–N bond cleavage in methylamine-derived intermediates on Pt(111) surface. Calculated $\Delta H^{\ddagger}$ and $\Delta G^{\ddagger}$ values are shown in Table S2. Structures and their reaction mode files (POSCAR and MODECAR files) are available in the supporting information.

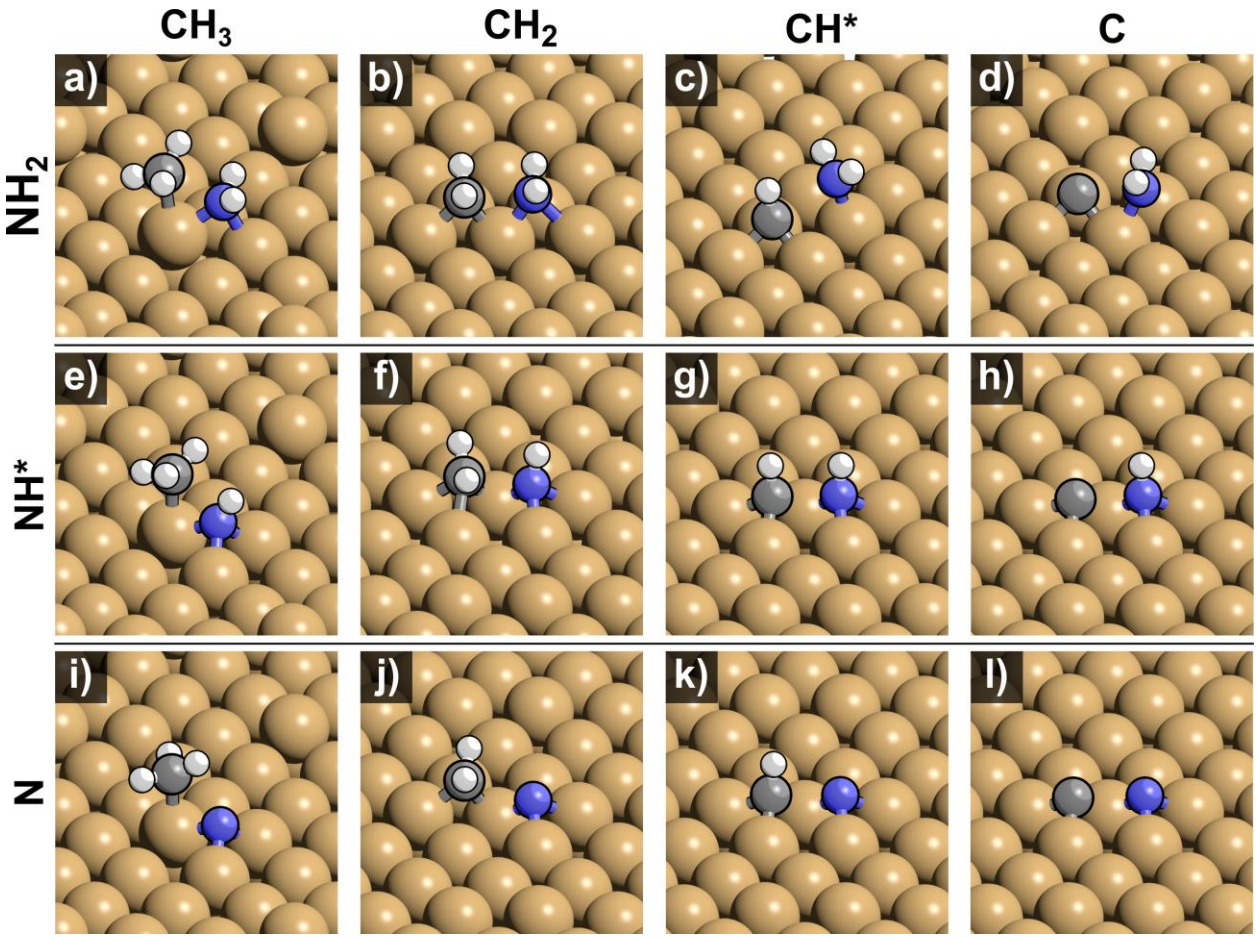

Figure S26. Transition state structures for C–N bond cleavage in methylamine-derived intermediates on Cu(111) surface. Calculated $\Delta H^{\neq}$ and $\Delta G^{\neq}$ values are shown in Table S2. Structures and their reaction mode files (POSCAR and MODECAR files) are available in the supporting information.

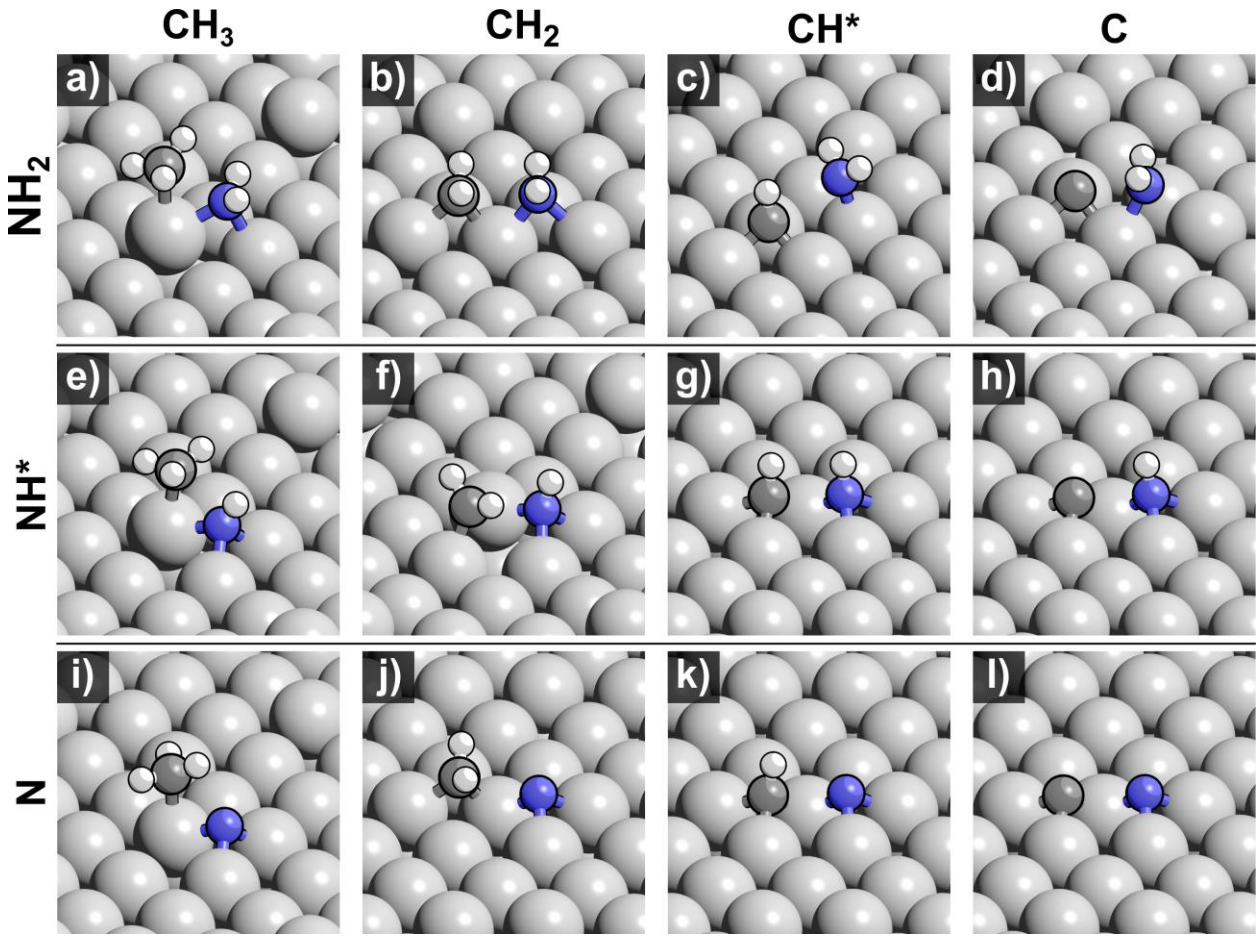

Figure S27. Transition state structures for C–N bond cleavage in methylamine-derived intermediates on Ag(111) surface. Calculated $\Delta H^{\neq}$ and $\Delta G^{\neq}$ values are shown in Table S2. Structures and their reaction mode files (POSCAR and MODECAR files) are available in the supporting information.

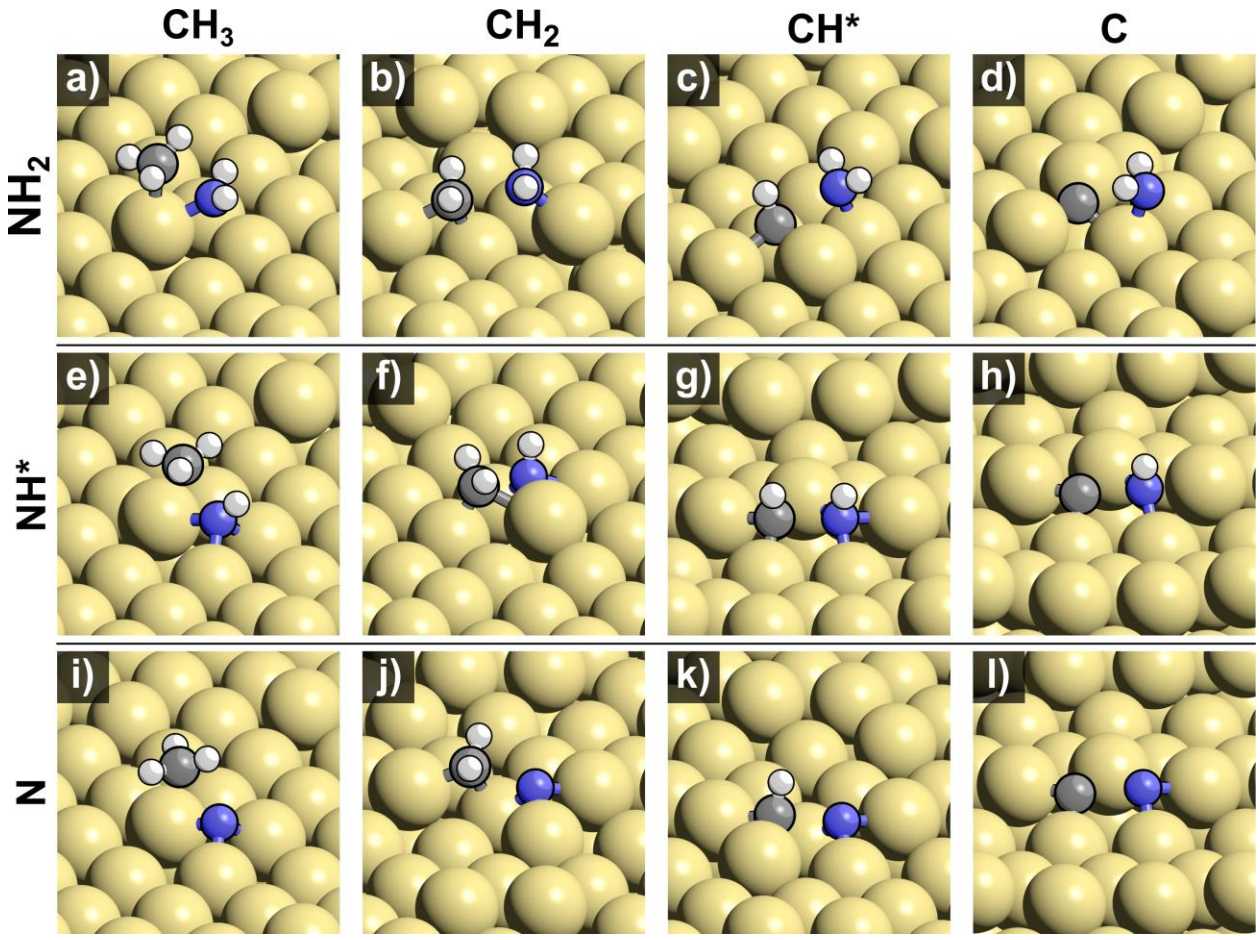

Figure S28. Transition state structures for C–N bond cleavage in methylamine-derived intermediates on Au(111) surface. Calculated $\Delta H^{\neq}$ and $\Delta G^{\neq}$ values are shown in Table S2. Structures and their reaction mode files (POSCAR and MODECAR files) are available in the supporting information.

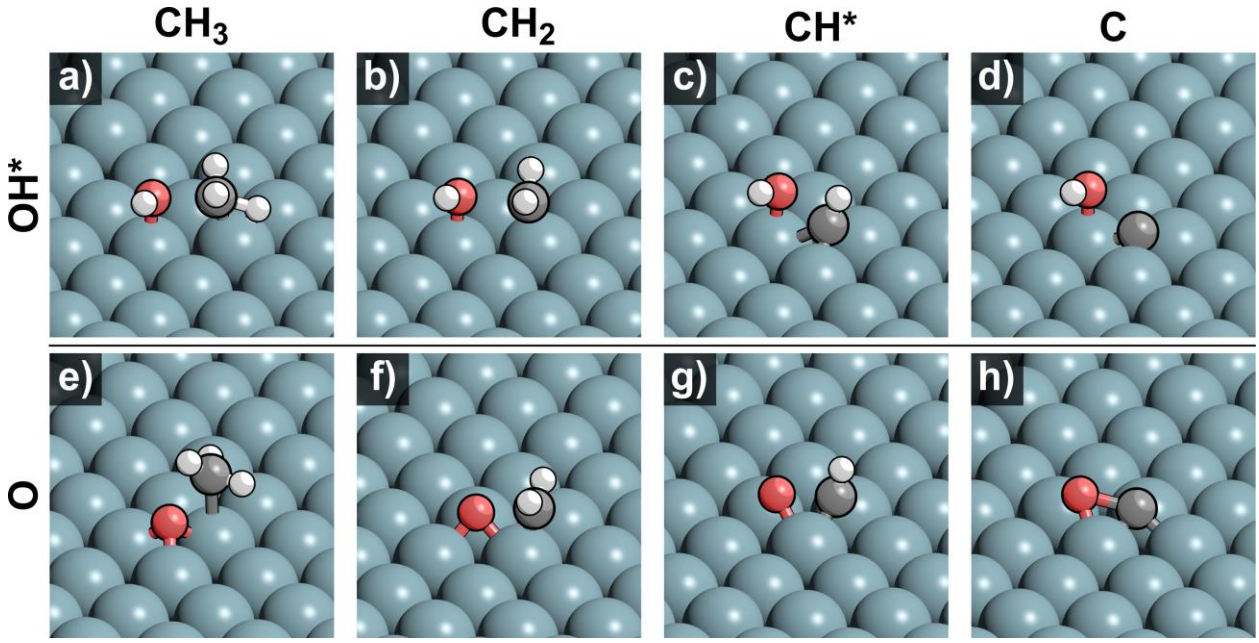

Figure S29. Transition state structures for C–O bond cleavage in methanol-derived intermediates on Ru(001) surface. Calculated $\Delta H^{\neq}$ and $\Delta G^{\neq}$ values are shown in Table S3. Structures and their reaction mode files (POSCAR and MODECAR files) are available in the supporting information.

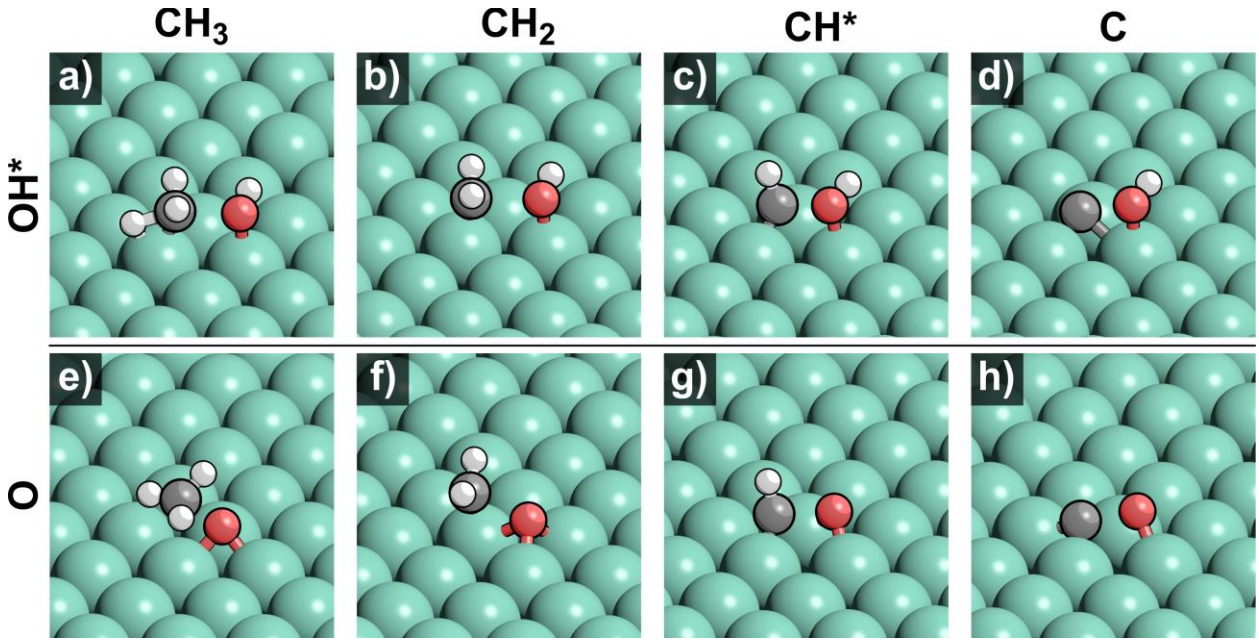

Figure S30. Transition state structures for C–O bond cleavage in methanol-derived intermediates on Os(001) surface. Calculated $\Delta H^{\neq}$ and $\Delta G^{\neq}$ values are shown in Table S3. Structures and their reaction mode files (POSCAR and MODECAR files) are available in the supporting information.

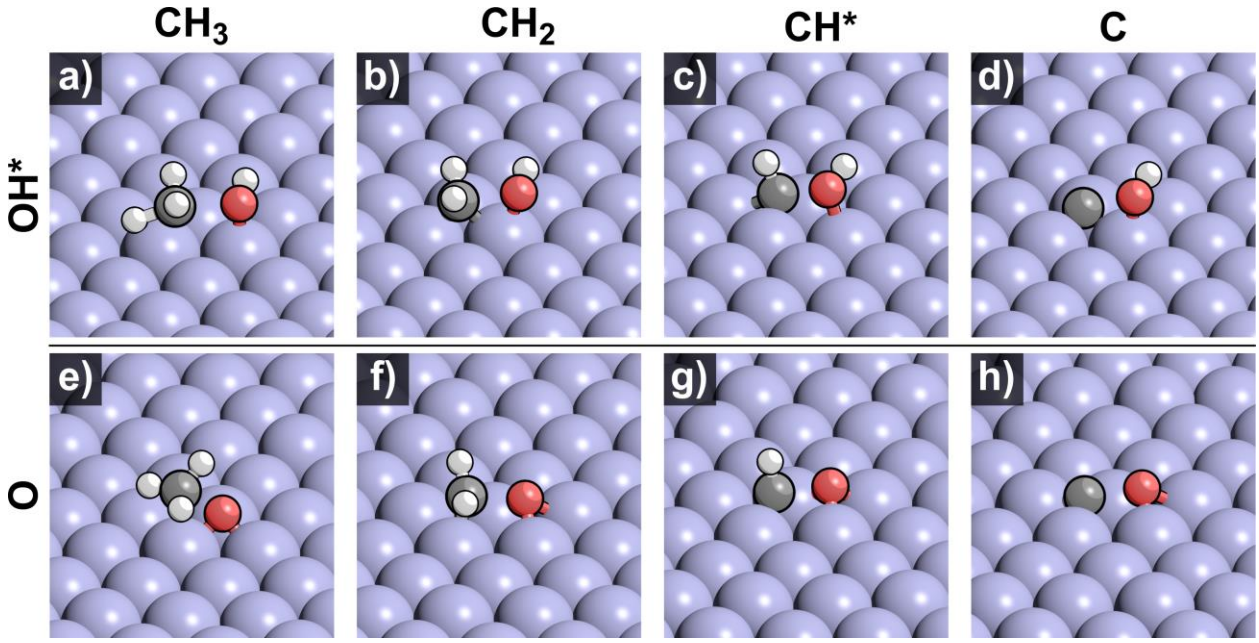

Figure S31. Transition state structures for C–O bond cleavage in methanol-derived intermediates on Co(001) surface. Calculated $\Delta H^{\neq}$ and $\Delta G^{\neq}$ values are shown in Table S3. Structures and their reaction mode files (POSCAR and MODECAR files) are available in the supporting information.

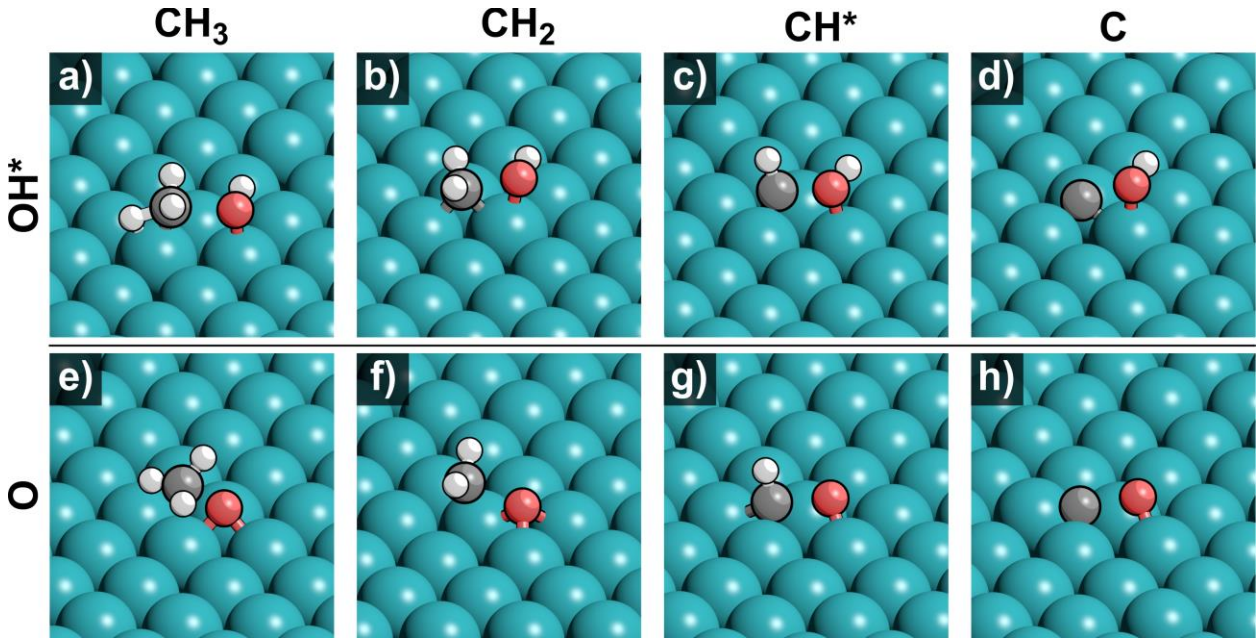

Figure S32. Transition state structures for C–O bond cleavage in methanol-derived intermediates on Rh(111) surface. Calculated $\Delta H^{\neq}$ and $\Delta G^{\neq}$ values are shown in Table S3. Structures and their reaction mode files (POSCAR and MODECAR files) are available in the supporting information.

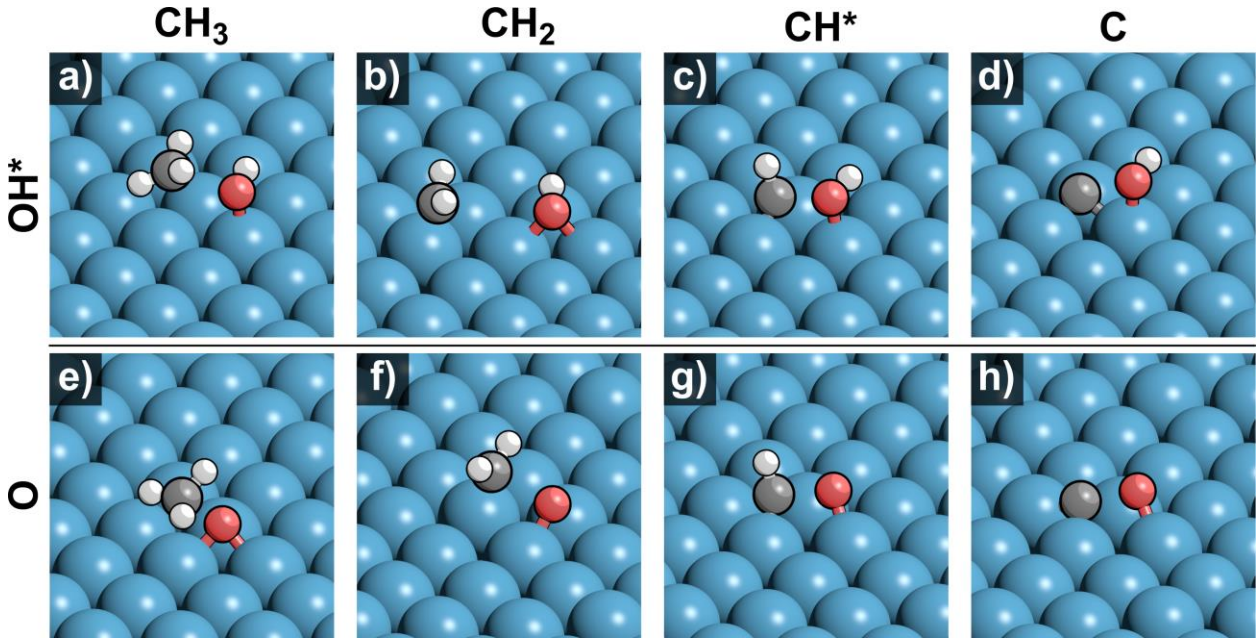

Figure S33. Transition state structures for C–O bond cleavage in methanol-derived intermediates on Ir(111) surface. Calculated $\Delta H^{\ddagger}$ and $\Delta G^{\ddagger}$ values are shown in Table S3. Structures and their reaction mode files (POSCAR and MODECAR files) are available in the supporting information.

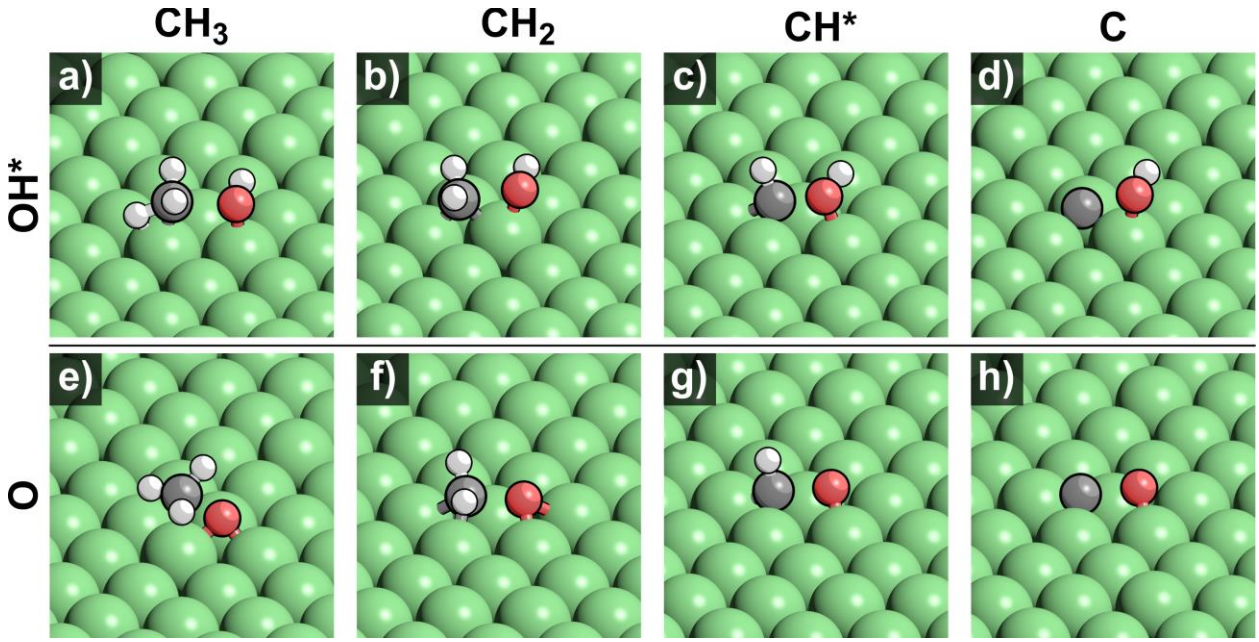

Figure S34. Transition state structures for C–O bond cleavage in methanol-derived intermediates on Ni(111) surface. Calculated $\Delta H^{\ddagger}$ and $\Delta G^{\ddagger}$ values are shown in Table S3. Structures and their reaction mode files (POSCAR and MODECAR files) are available in the supporting information.

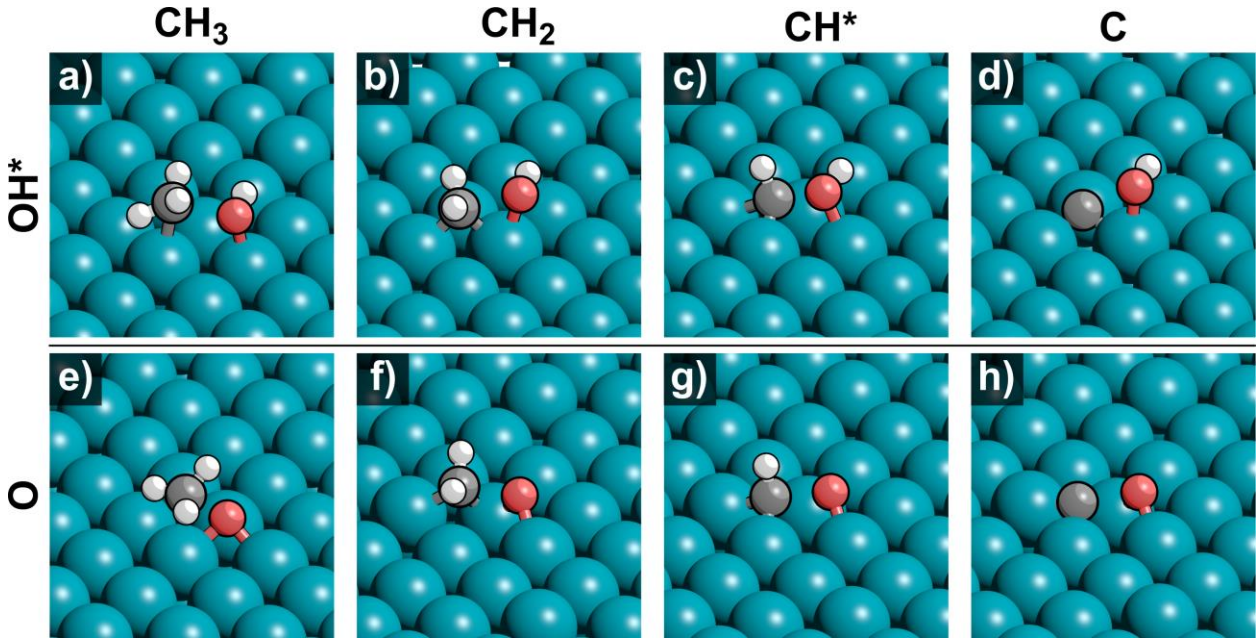

Figure S35. Transition state structures for C–O bond cleavage in methanol-derived intermediates on Pd(111) surface. Calculated $\Delta H^{\neq}$ and $\Delta G^{\neq}$ values are shown in Table S3. Structures and their reaction mode files (POSCAR and MODECAR files) are available in the supporting information.

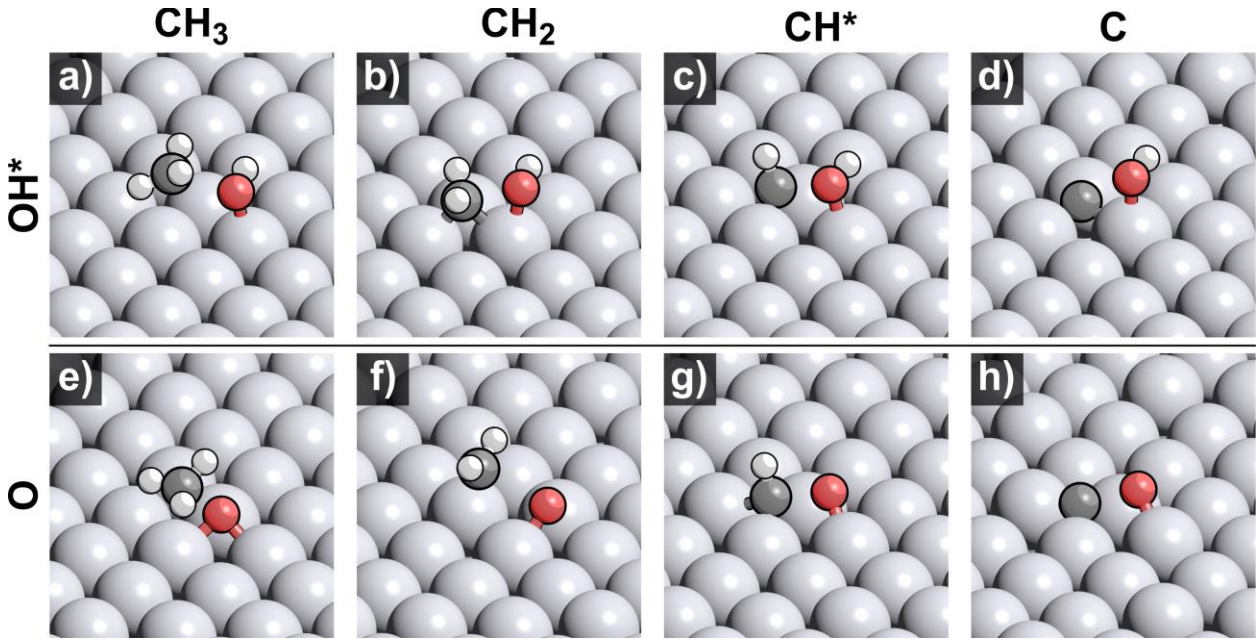

Figure S36. Transition state structures for C–O bond cleavage in methanol-derived intermediates on Pt(111) surface. Calculated $\Delta H^{\neq}$ and $\Delta G^{\neq}$ values are shown in Table S3. Structures and their reaction mode files (POSCAR and MODECAR files) are available in the supporting information.

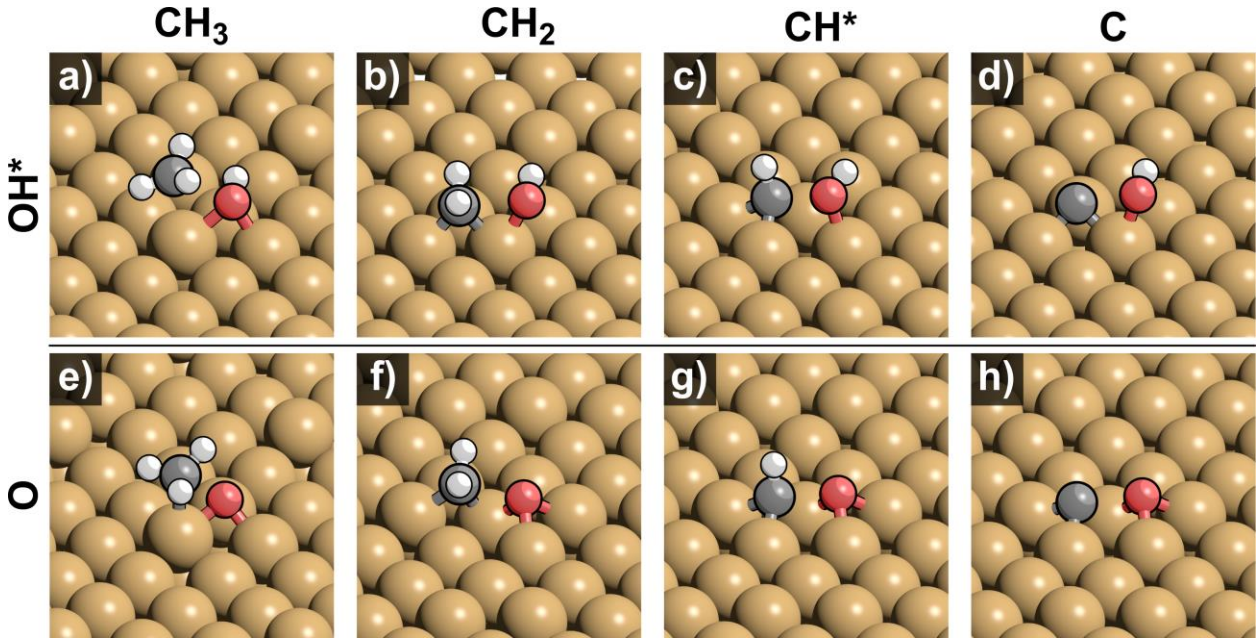

Figure S37. Transition state structures for C–O bond cleavage in methanol-derived intermediates on Cu(111) surface. Calculated $\Delta H^{\neq}$ and $\Delta G^{\neq}$ values are shown in Table S3. Structures and their reaction mode files (POSCAR and MODECAR files) are available in the supporting information.

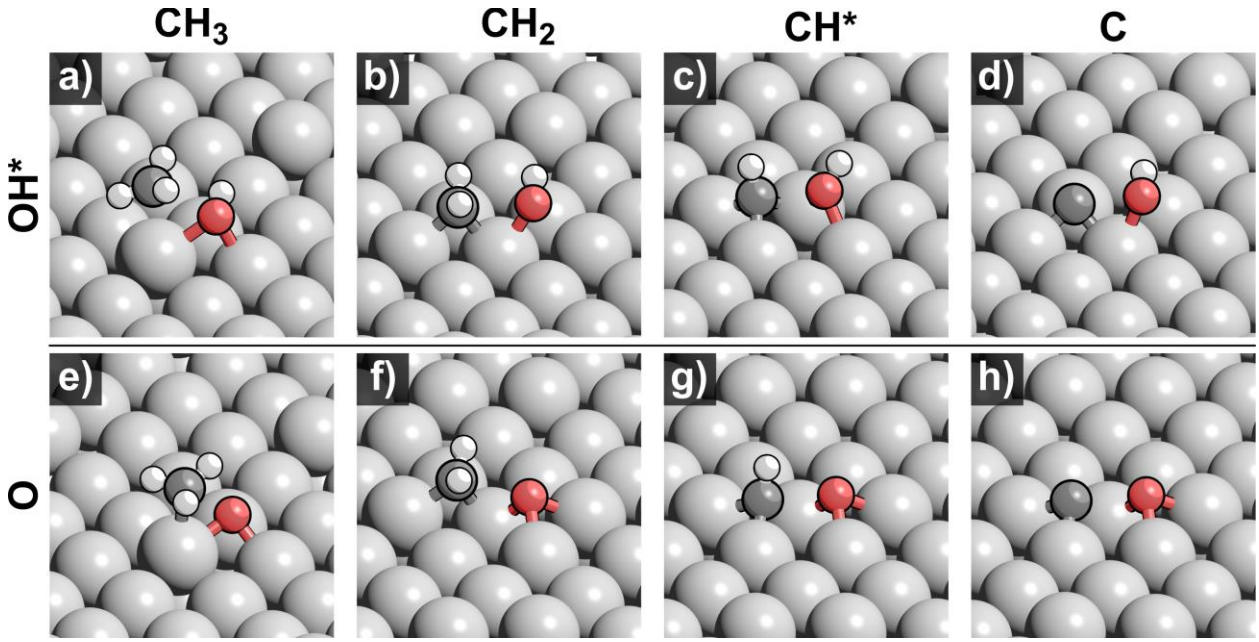

Figure S38. Transition state structures for C–O bond cleavage in methanol-derived intermediates on Ag(111) surface. Calculated $\Delta H^{\neq}$ and $\Delta G^{\neq}$ values are shown in Table S3. Structures and their reaction mode files (POSCAR and MODECAR files) are available in the supporting information.

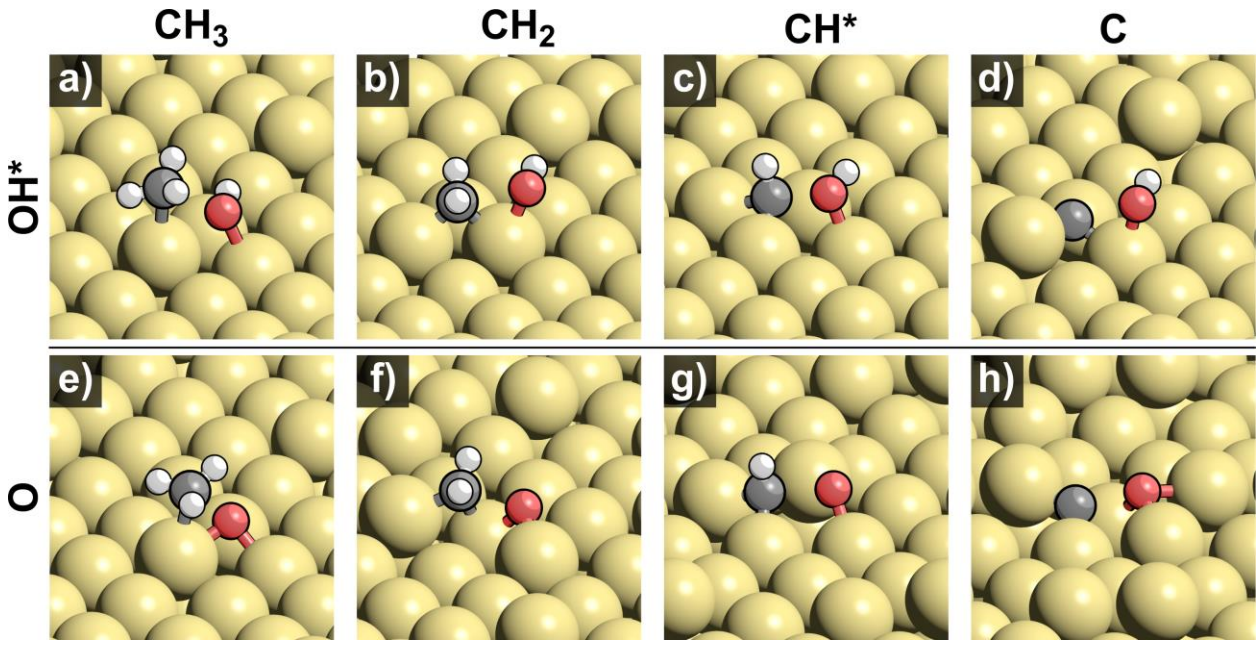

Figure S39. Transition state structures for C–O bond cleavage in methanol-derived intermediates on Au(111) surface. Calculated $\Delta H^{\neq}$ and $\Delta G^{\neq}$ values are shown in Table S3. Structures and their reaction mode files (POSCAR and MODECAR files) are available in the supporting information.

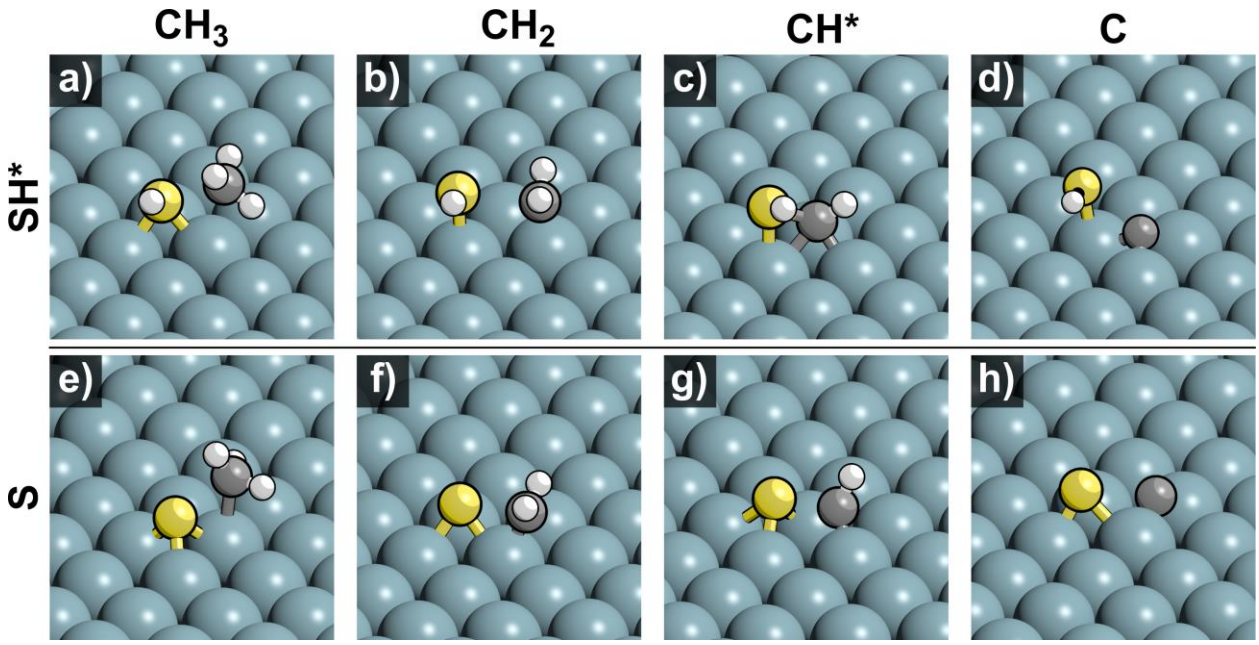

Figure S40. Transition state structures for C–S bond cleavage in methanethiol-derived intermediates on Ru(001) surface. Calculated $\Delta H^{\ddagger}$ and $\Delta G^{\ddagger}$ values are shown in Table S3. Structures and their reaction mode files (POSCAR and MODECAR files) are available in the supporting information.

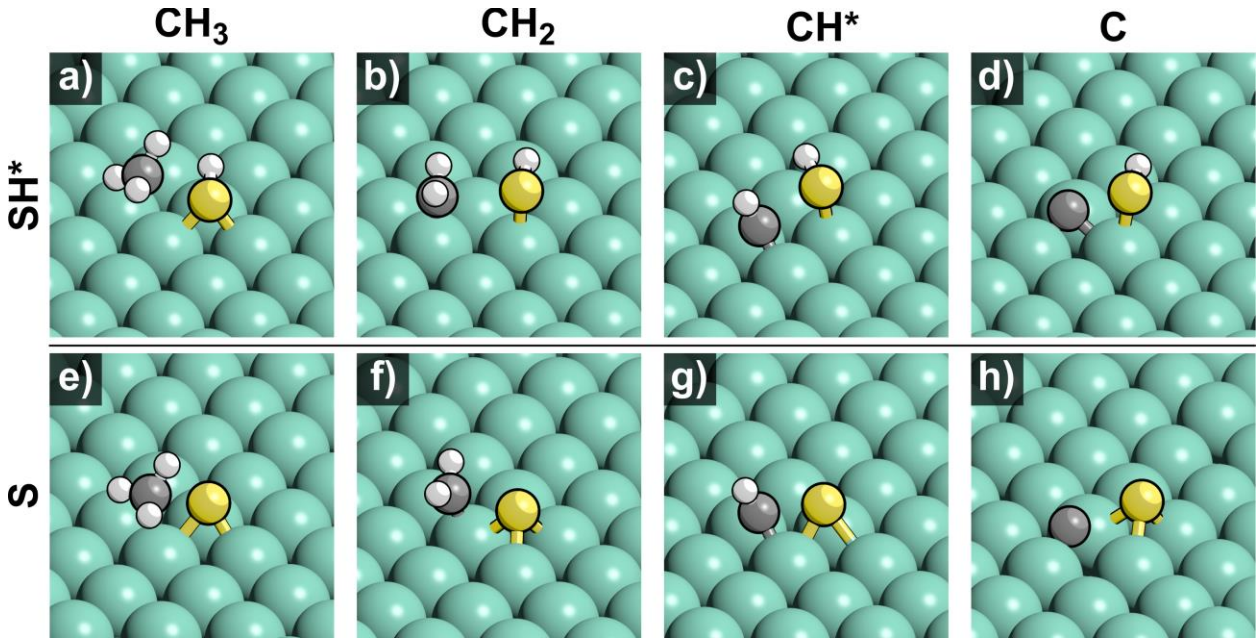

Figure S41. Transition state structures for C–S bond cleavage in methanethiol-derived intermediates on Os(001) surface. Calculated $\Delta H^{\ddagger}$ and $\Delta G^{\ddagger}$ values are shown in Table S3. Structures and their reaction mode files (POSCAR and MODECAR files) are available in the supporting information.

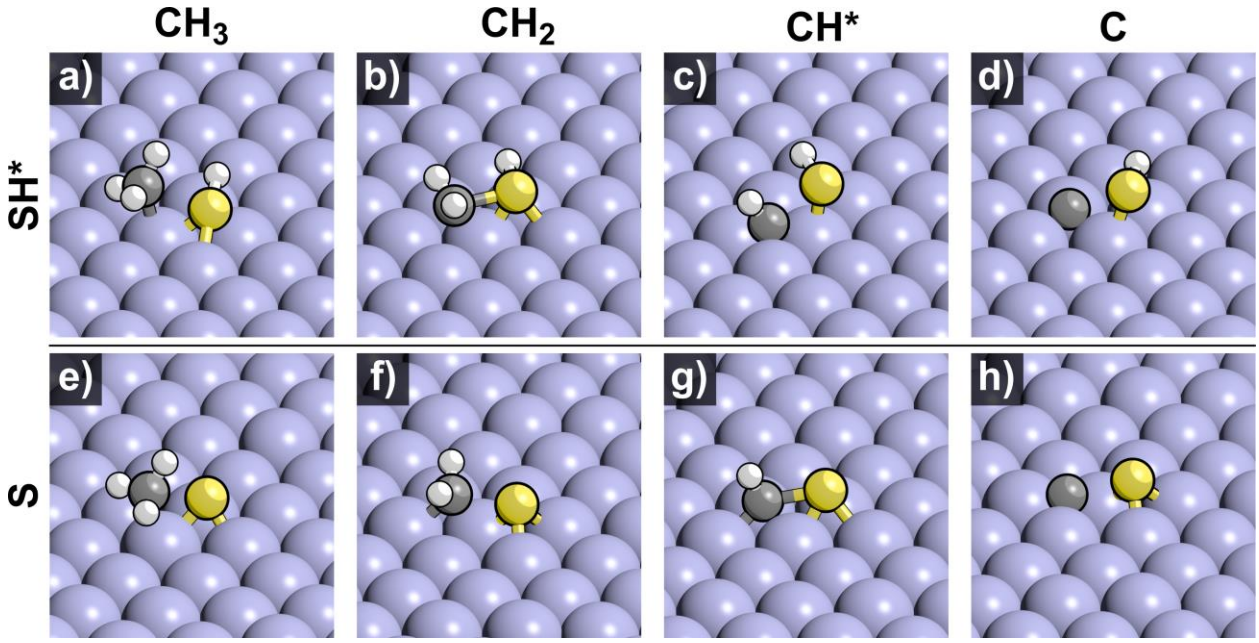

Figure S42. Transition state structures for C–S bond cleavage in methanethiol-derived intermediates on Co(001) surface. Calculated $\Delta H^{\neq}$ and $\Delta G^{\neq}$ values are shown in Table S3. Structures and their reaction mode files (POSCAR and MODECAR files) are available in the supporting information.

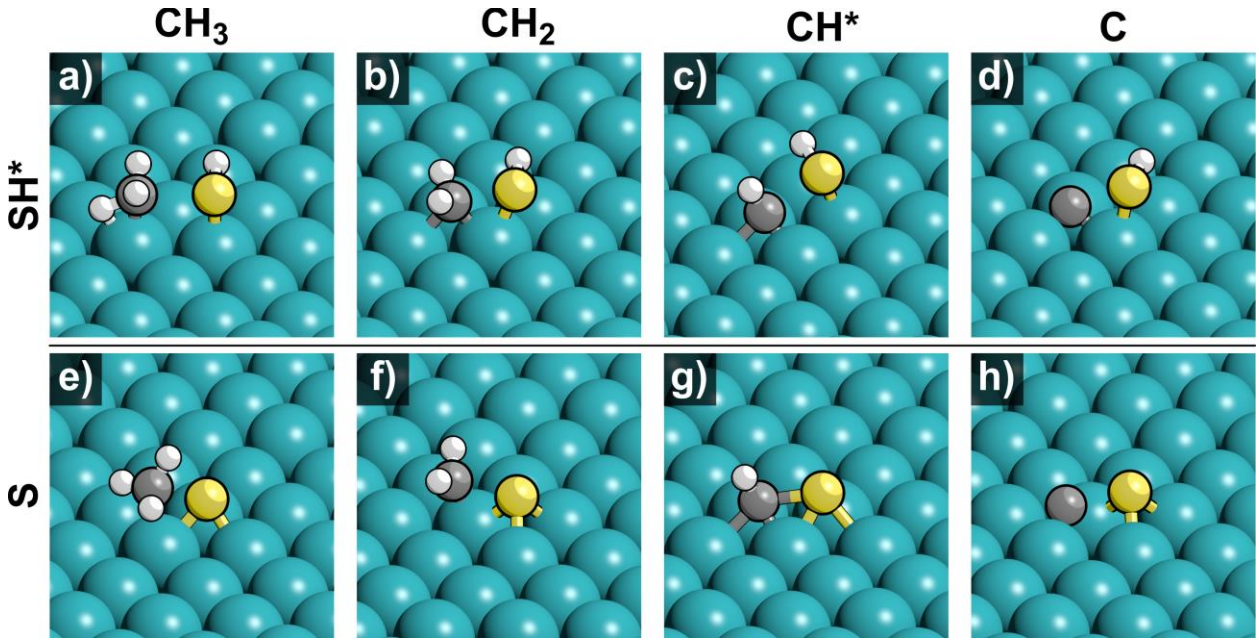

Figure S43. Transition state structures for C–S bond cleavage in methanethiol-derived intermediates on Rh(111) surface. Calculated $\Delta H^{\neq}$ and $\Delta G^{\neq}$ values are shown in Table S3. Structures and their reaction mode files (POSCAR and MODECAR files) are available in the supporting information.

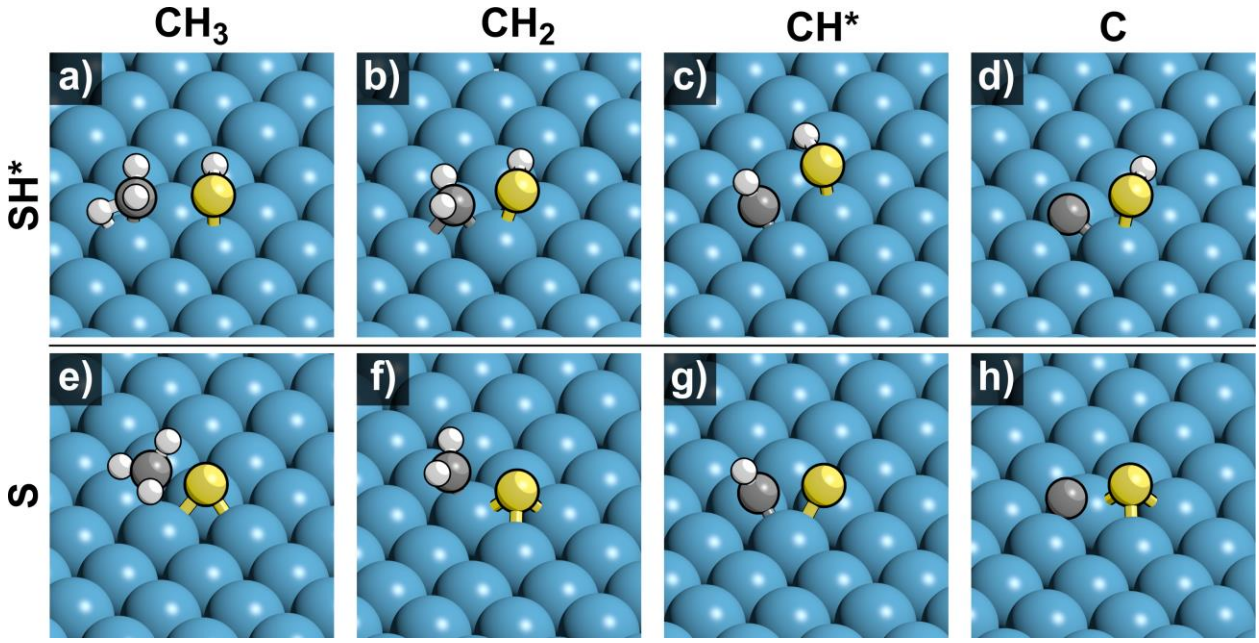

Figure S44. Transition state structures for C–S bond cleavage in methanethiol-derived intermediates on Ir(111) surface. Calculated $\Delta H^{\ddagger}$ and $\Delta G^{\ddagger}$ values are shown in Table S3. Structures and their reaction mode files (POSCAR and MODECAR files) are available in the supporting information.

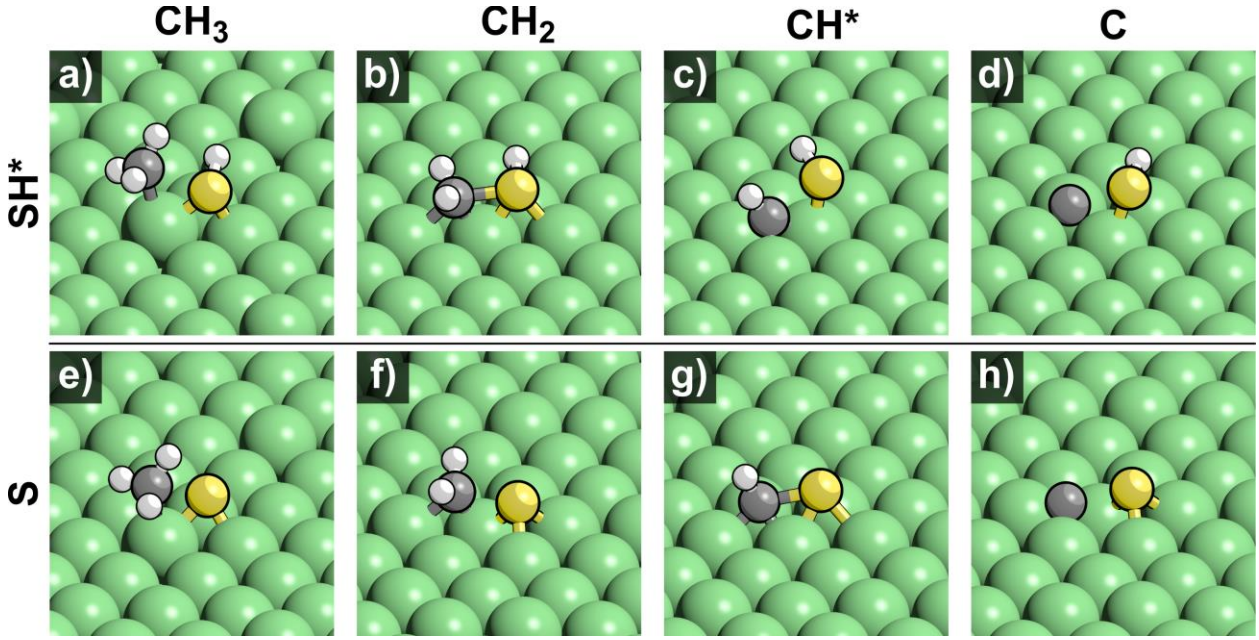

Figure S45. Transition state structures for C–S bond cleavage in methanethiol-derived intermediates on Ni(111) surface. Calculated $\Delta H^{\ddagger}$ and $\Delta G^{\ddagger}$ values are shown in Table S3. Structures and their reaction mode files (POSCAR and MODECAR files) are available in the supporting information.

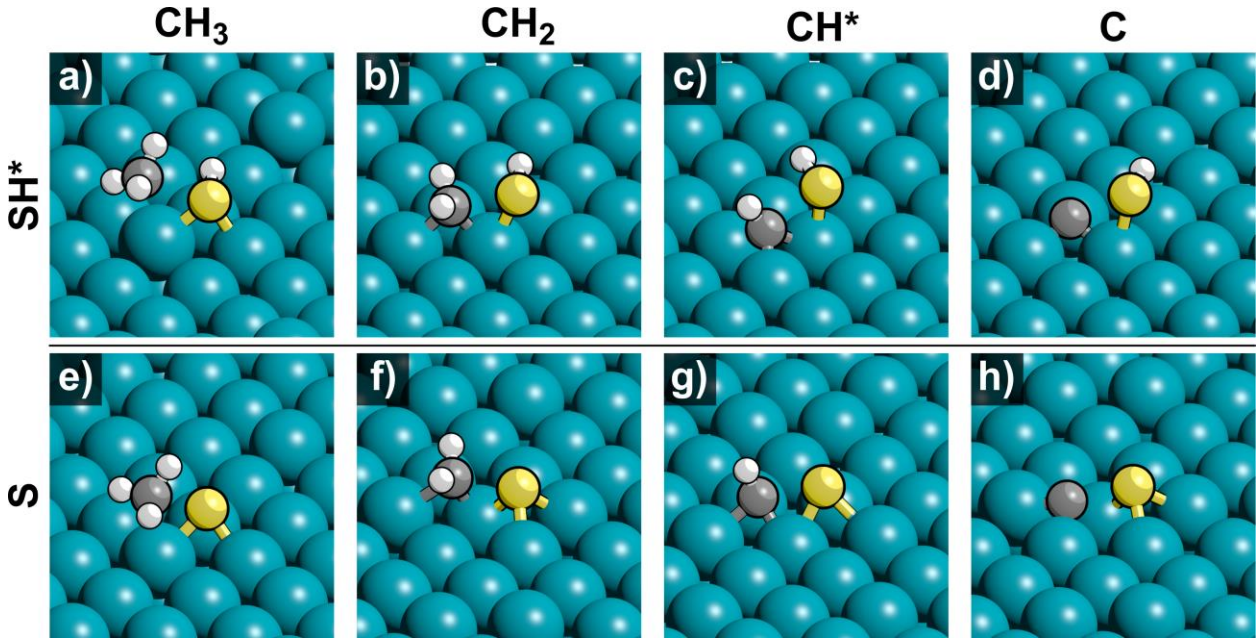

Figure S46. Transition state structures for C–S bond cleavage in methanethiol-derived intermediates on Pd(111) surface. Calculated $\Delta H^{\ddagger}$ and $\Delta G^{\ddagger}$ values are shown in Table S3. Structures and their reaction mode files (POSCAR and MODECAR files) are available in the supporting information.

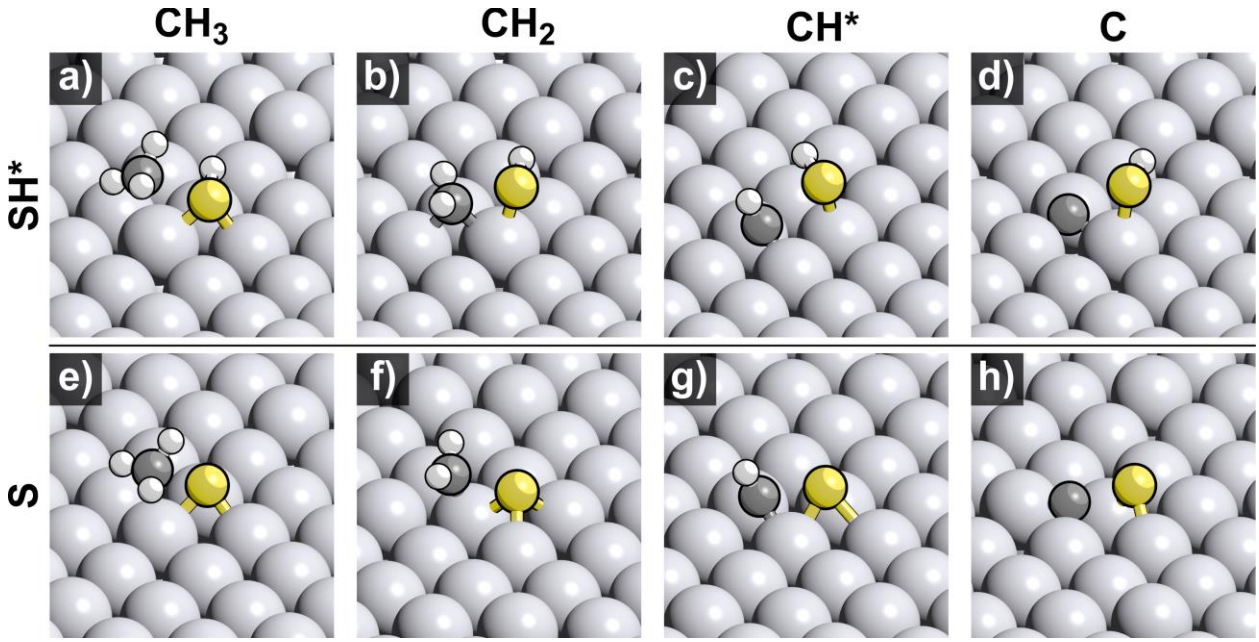

Figure S47. Transition state structures for C–S bond cleavage in methanethiol-derived intermediates on Pt(111) surface. Calculated $\Delta H^{\ddagger}$ and $\Delta G^{\ddagger}$ values are shown in Table S3. Structures and their reaction mode files (POSCAR and MODECAR files) are available in the supporting information.

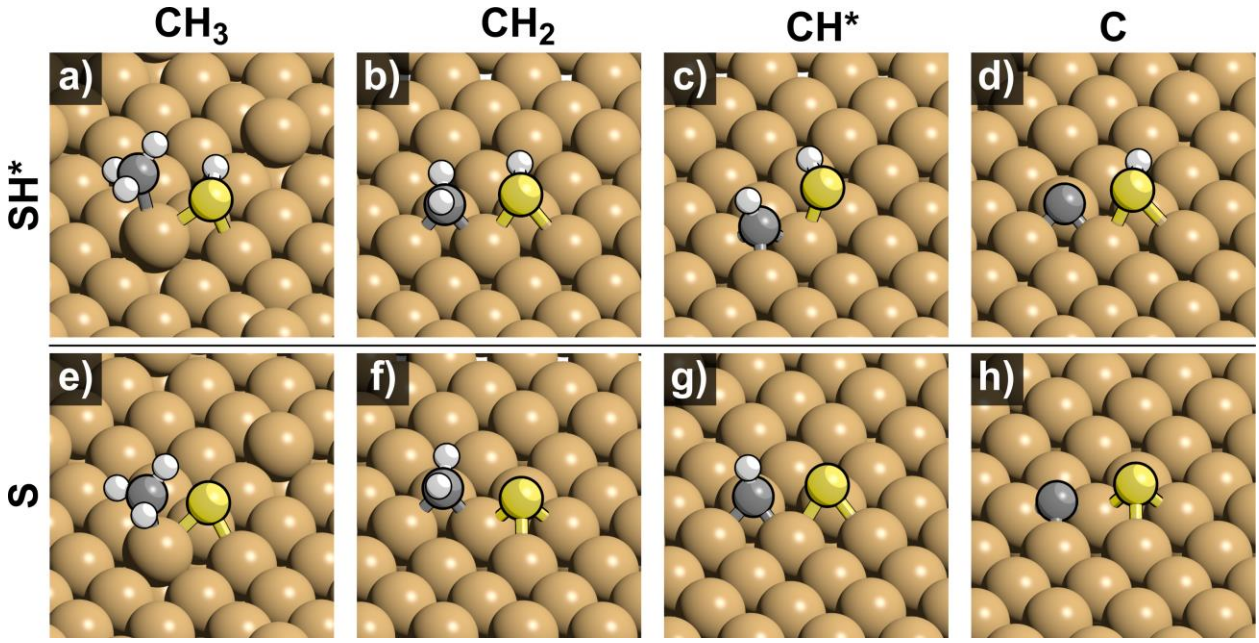

Figure S48. Transition state structures for C–S bond cleavage in methanethiol-derived intermediates on Cu(111) surface. Calculated $\Delta H^{\ddagger}$ and $\Delta G^{\ddagger}$ values are shown in Table S3. Structures and their reaction mode files (POSCAR and MODECAR files) are available in the supporting information.

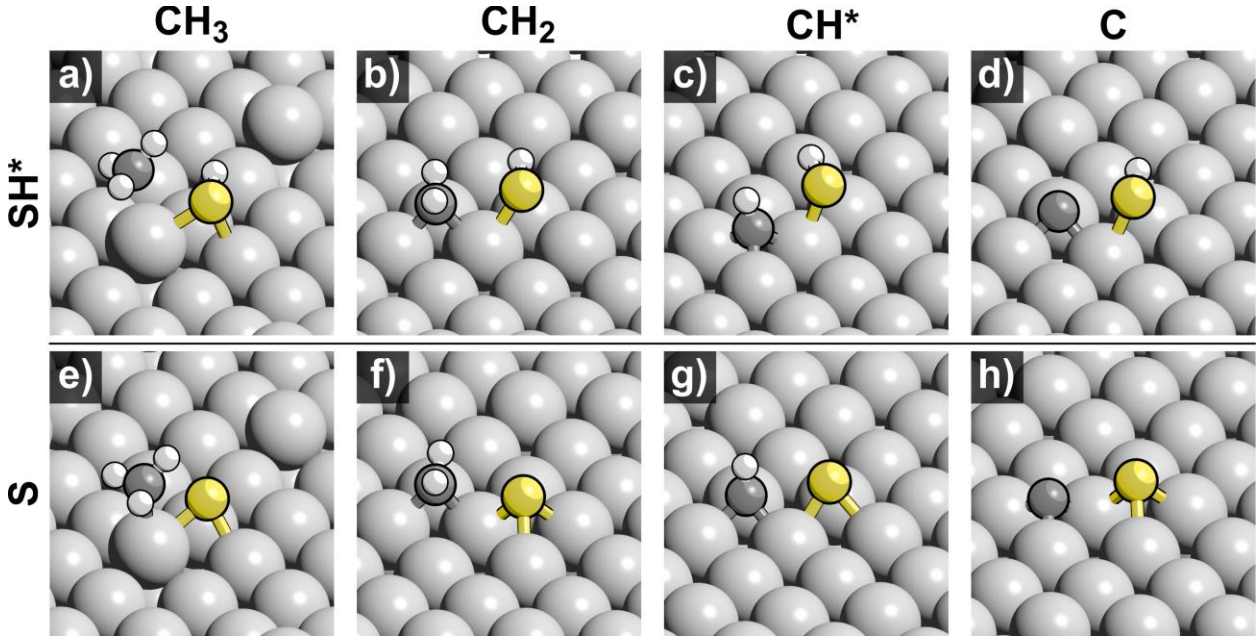

Figure S49. Transition state structures for C–S bond cleavage in methanethiol-derived intermediates on Ag(111) surface. Calculated $\Delta H^{\ddagger}$ and $\Delta G^{\ddagger}$ values are shown in Table S3. Structures and their reaction mode files (POSCAR and MODECAR files) are available in the supporting information.

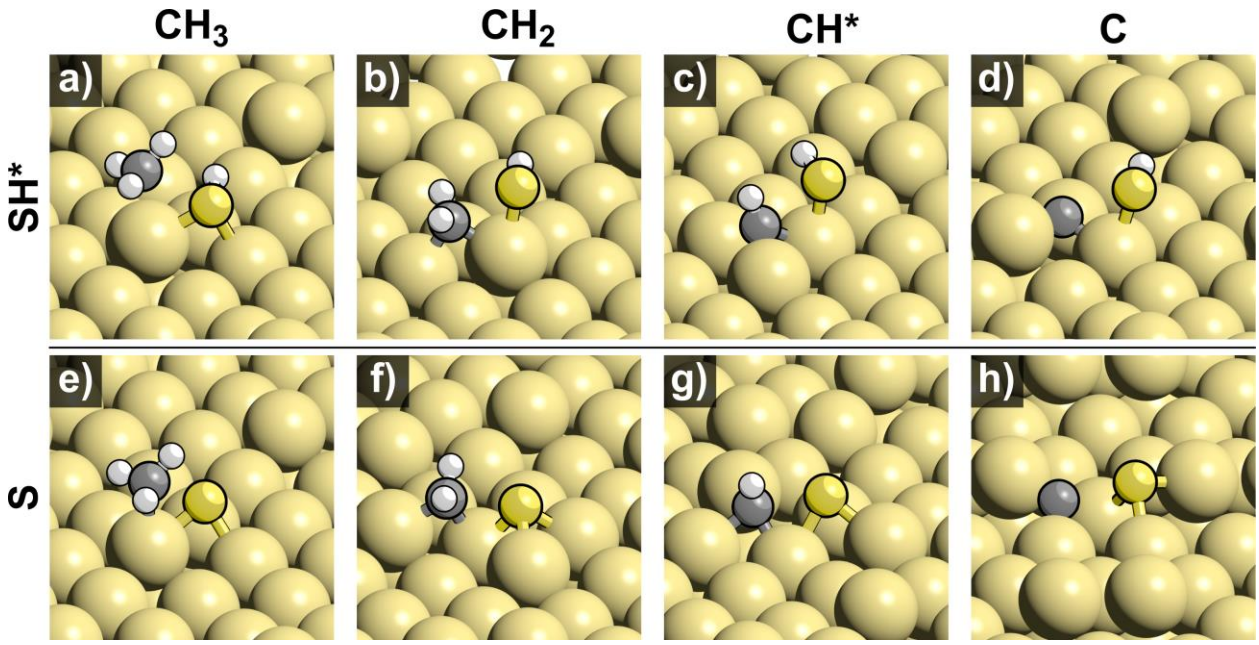

Figure S50. Transition state structures for C–S bond cleavage in methanethiol-derived intermediates on Au(111) surface. Calculated $\Delta H^{\ddagger}$ and $\Delta G^{\ddagger}$ values are shown in Table S3. Structures and their reaction mode files (POSCAR and MODECAR files) are available in the supporting information.

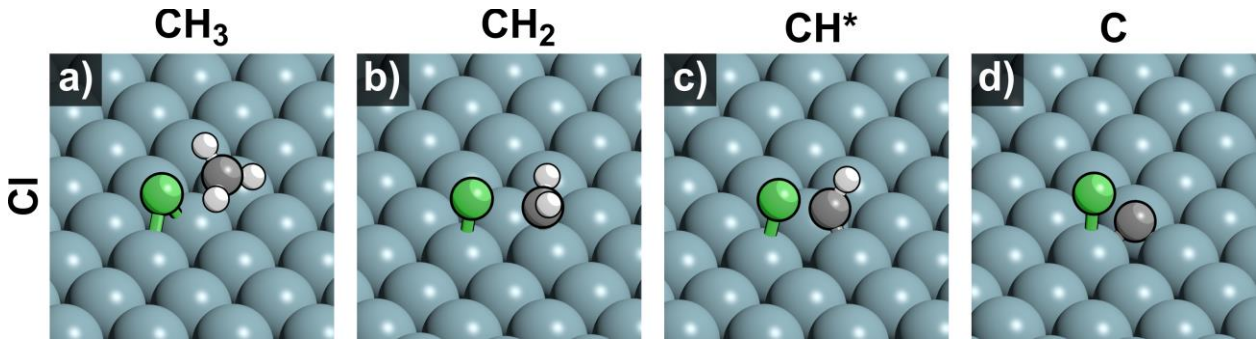

Figure S51. Transition state structures for C–Cl bond cleavage in chloromethane-derived intermediates on Ru(001) surface. Calculated $\Delta H^{\ddagger}$ and $\Delta G^{\ddagger}$ values are shown in Table S4. Structures and their reaction mode files (POSCAR and MODECAR files) are available in the supporting information.

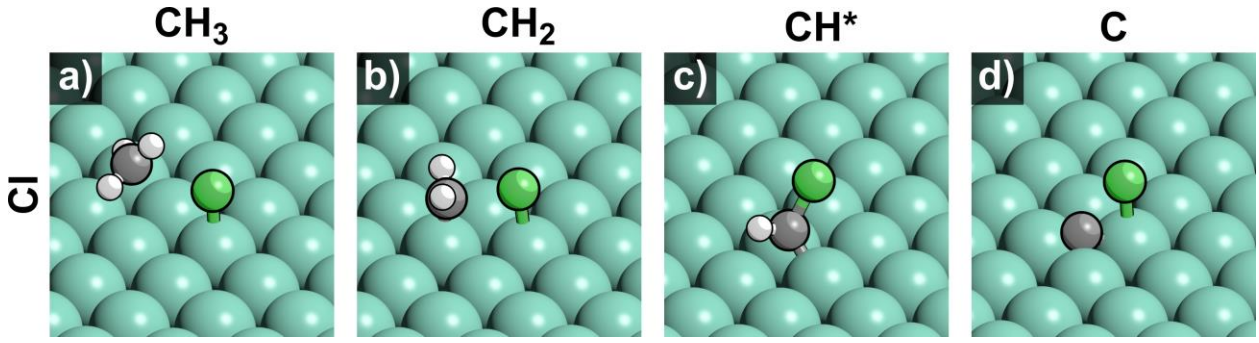

Figure S52. Transition state structures for C–Cl bond cleavage in chloromethane-derived intermediates on Os(001) surface. Calculated $\Delta H^{\ddagger}$ and $\Delta G^{\ddagger}$ values are shown in Table S4. Structures and their reaction mode files (POSCAR and MODECAR files) are available in the supporting information.

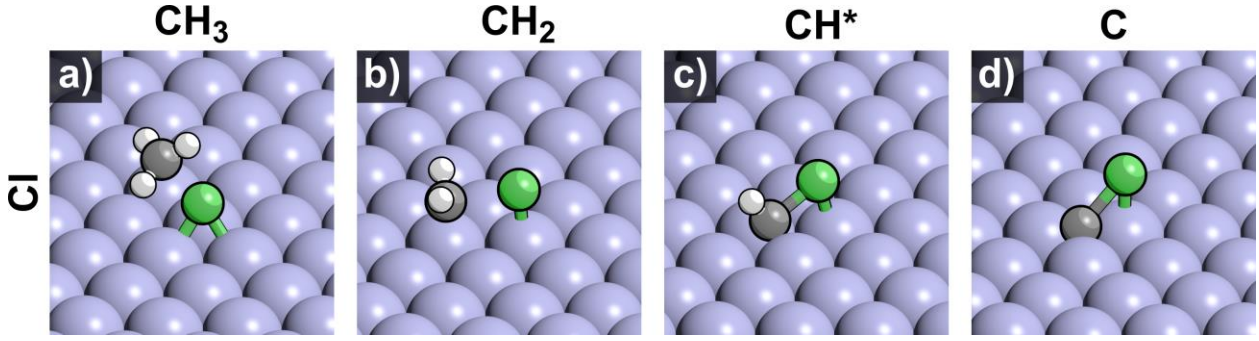

Figure S53. Transition state structures for C–Cl bond cleavage in chloromethane-derived intermediates on Co(001) surface. Calculated $\Delta H^{\ddagger}$ and $\Delta G^{\ddagger}$ values are shown in Table S4. Structures and their reaction mode files (POSCAR and MODECAR files) are available in the supporting information.

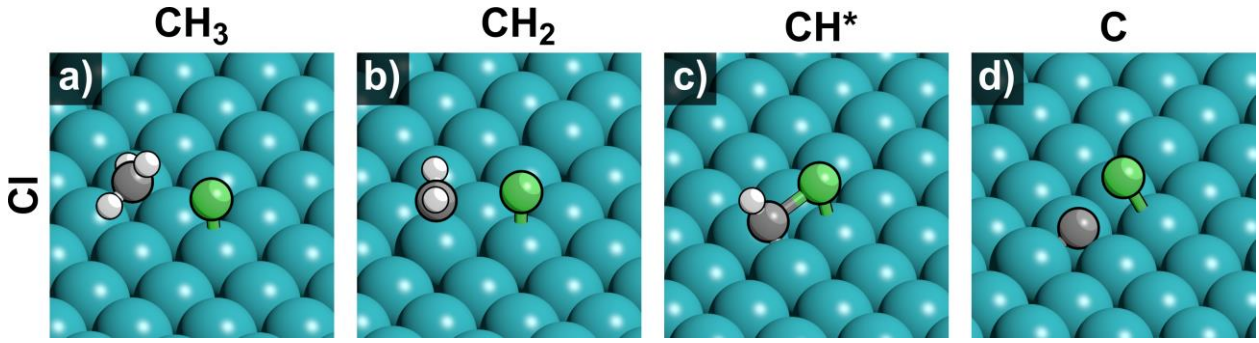

Figure S54. Transition state structures for C–Cl bond cleavage in chloromethane-derived intermediates on Rh(111) surface. Calculated $\Delta H^{\neq}$ and $\Delta G^{\neq}$ values are shown in Table S4. Structures and their reaction mode files (POSCAR and MODECAR files) are available in the supporting information.

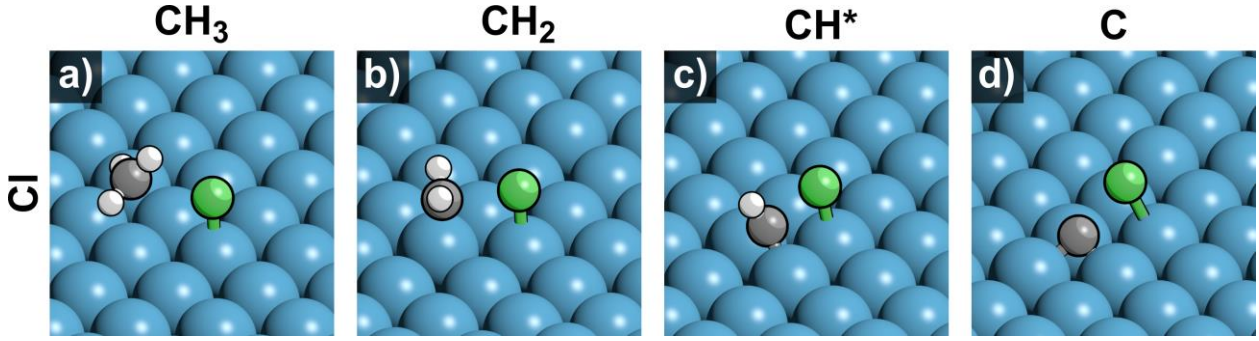

Figure S55. Transition state structures for C–Cl bond cleavage in chloromethane-derived intermediates on Ir(111) surface. Calculated $\Delta H^{\neq}$ and $\Delta G^{\neq}$ values are shown in Table S4. Structures and their reaction mode files (POSCAR and MODECAR files) are available in the supporting information.

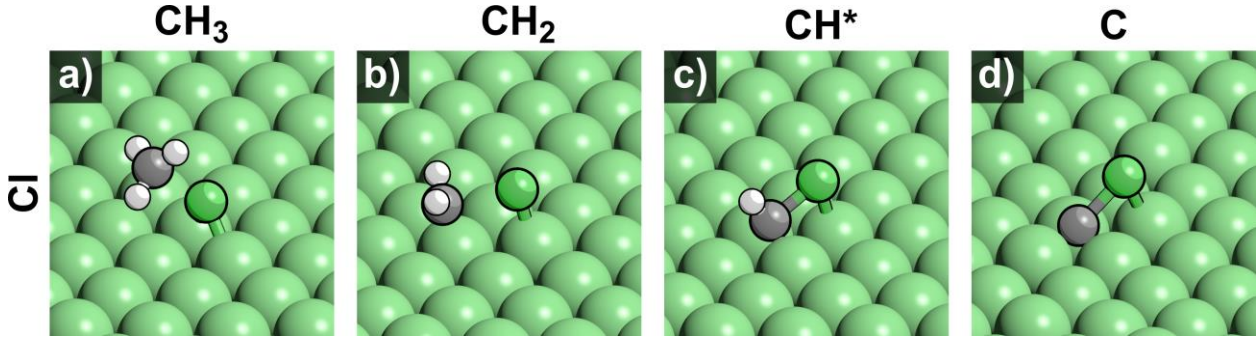

Figure S56. Transition state structures for C–Cl bond cleavage in chloromethane-derived intermediates on Ni(111) surface. Calculated $\Delta H^{\neq}$ and $\Delta G^{\neq}$ values are shown in Table S4. Structures and their reaction mode files (POSCAR and MODECAR files) are available in the supporting information.

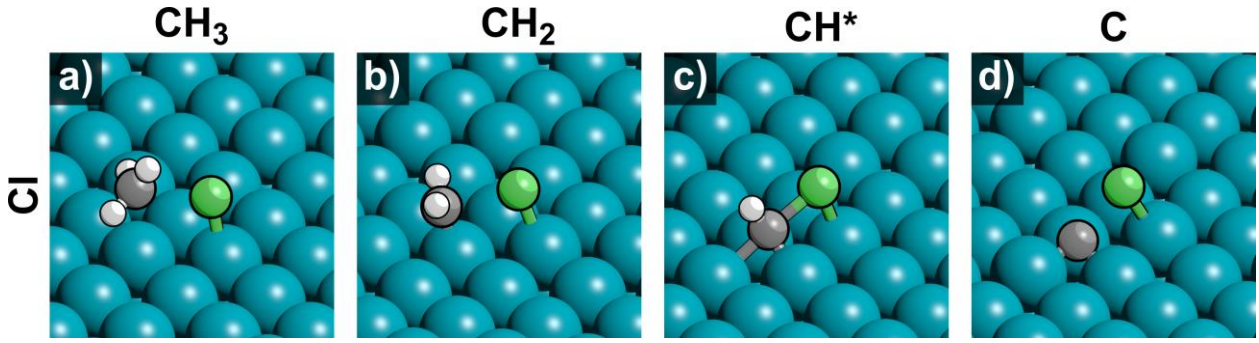

Figure S57. Transition state structures for C–Cl bond cleavage in chloromethane-derived intermediates on Pd(111) surface. Calculated $\Delta H^{\neq}$ and $\Delta G^{\neq}$ values are shown in Table S4. Structures and their reaction mode files (POSCAR and MODECAR files) are available in the supporting information.

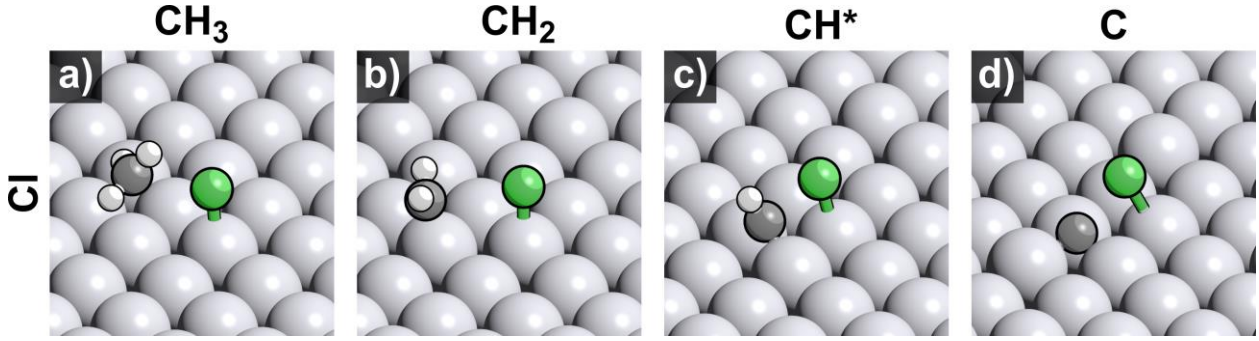

Figure S58. Transition state structures for C–Cl bond cleavage in chloromethane-derived intermediates on Pt(111) surface. Calculated $\Delta H^{\neq}$ and $\Delta G^{\neq}$ values are shown in Table S4. Structures and their reaction mode files (POSCAR and MODECAR files) are available in the supporting information.

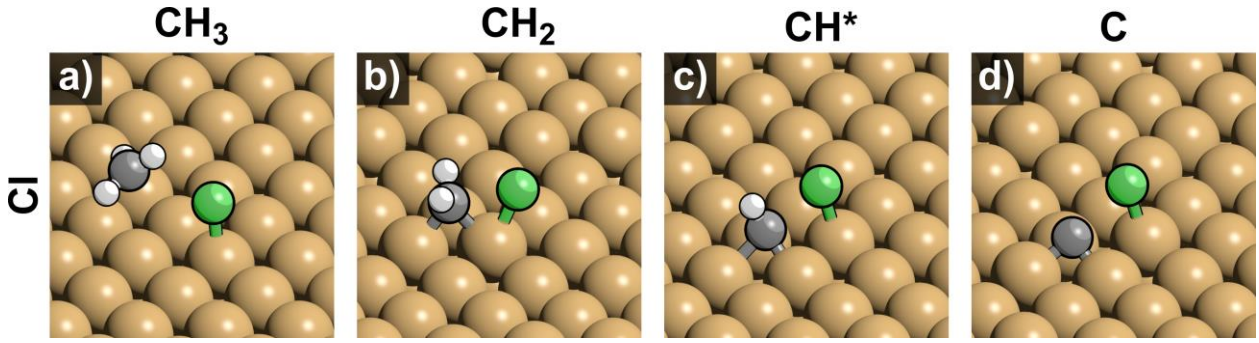

Figure S59. Transition state structures for C–Cl bond cleavage in chloromethane-derived intermediates on Cu(111) surface. Calculated $\Delta H^{\neq}$ and $\Delta G^{\neq}$ values are shown in Table S4. Structures and their reaction mode files (POSCAR and MODECAR files) are available in the supporting information.

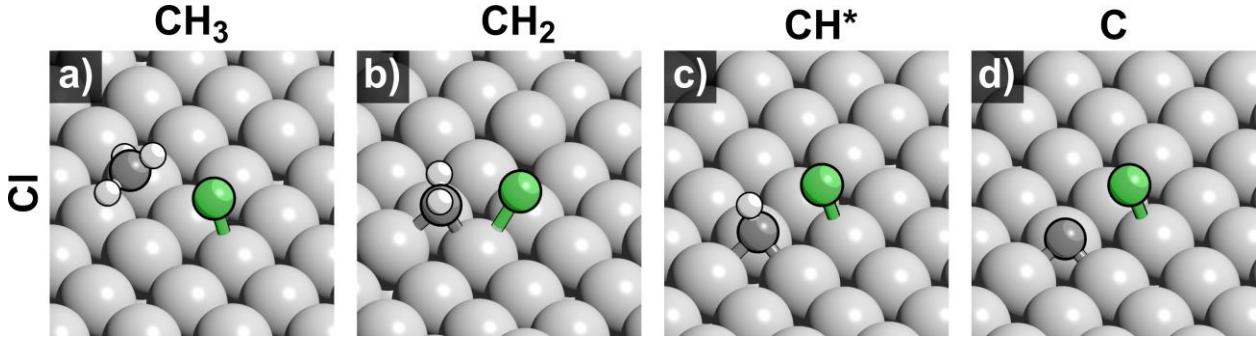

Figure S60. Transition state structures for C–Cl bond cleavage in chloromethane-derived intermediates on Ag(111) surface. Calculated $\Delta H^{\neq}$ and $\Delta G^{\neq}$ values are shown in Table S4. Structures and their reaction mode files (POSCAR and MODECAR files) are available in the supporting information.

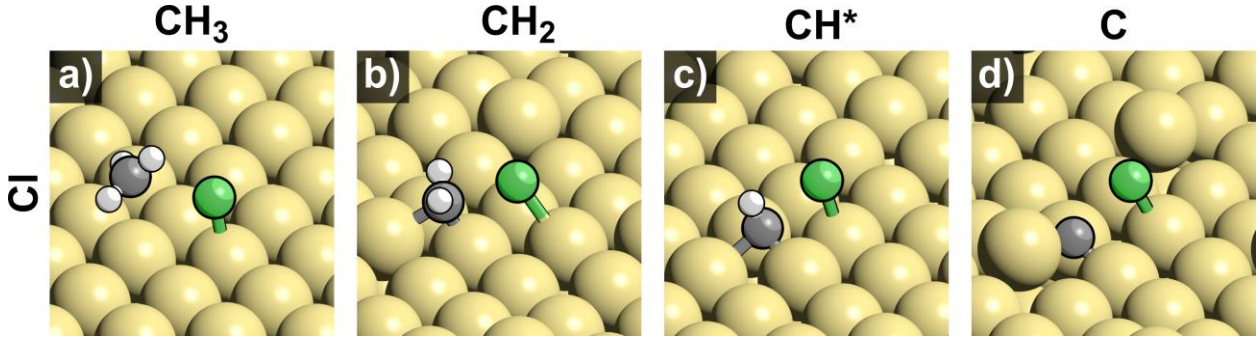

Figure S61. Transition state structures for C–Cl bond cleavage in chloromethane-derived intermediates on Au(111) surface. Calculated $\Delta H^{\neq}$ and $\Delta G^{\neq}$ values are shown in Table S4. Structures and their reaction mode files (POSCAR and MODECAR files) are available in the supporting information.